Table 2 Randomized, double-blind, placebo-controlled, crossover trial of HEW in 10 DM and 12 MM patients

	Dermatomyositis (DM)				Mitochondrial myopathies (MM)			
	Hydrogen water		Placebo water		Hydrogen water		Placebo water	
	0 week	8 weeks	0 week	8 weeks	0 week	8 weeks	0 week	8 weeks
CK (U/L)	88.7 ± 24.3	106.1 ± 88.2	93.5 ± 45.0	99.5 ± 86.7	165 ± 86.6	120 ± 55.5	142.0 ± 69.4	221 ± 235
HbA1c (%)	6.23 ± 1.28	6.34 ± 1.55	6.27 ± 1.44	6.16 ± 1.28	6.09 ± 0.94	6.12 ± 1.05	6.06 ± 1.22	6.06 ± 1.02
Fasting glucose (mmol/L)	8.27 ± 3.62	7.81 ± 2.91	6.70 ± 2.11	6.48 ± 1.90	6.05 ± 1.43	5.67 ± 1.99	6.02 ± 1.46	6.11 ± 1.69
Lactate (mmol/L)	1.93 ± 0.78	1.81 ± 0.87	1.80 ± 0.89	1.65 ± 0.77	1.76 ± 0.67*	1.61 ± 0.48*	1.49 ± 0.49*	1.70 ± 0.57*
L/P ratio	13.1 ± 6.0	11.5 ± 2.6	12.1 ± 2.88	15.2 ± 8.3	18.7 ± 8.8	17.9 ± 7.7	7.12 ± 13.4	17.7 ± 8.6
Creatinine (μmol/L)	59.1 ± 15.6	59.1 ± 13.6	58.3 ± 15.0	59.0 ± 19.7	53.6 ± 18.3	52.0 ± 17.4	54.8 ± 20.3	57.5 ± 22.3
BUN (mmol/L)	5.36 ± 1.48	4.82 ± 1.57	5.78 ± 1.71	4.86 ± 1.56	6.08 ± 2.09	5.39 ± 1.54	6.24 ± 1.46	6.34 ± 2.76
Uric Acid (μmol/dL)	303 ± 88	320 ± 68	313 ± 75	321 ± 83	413 ± 316	375 ± 229	447 ± 387	408 ± 284
T-chol (mmol/L)	5.23 ± 0.78	5.15 ± 0.85	5.21 ± 0.61	4.95 ± 0.92	4.61 ± 0.78	4.80 ± 0.57	4.69 ± 0.78	4.68 ± 0.71
LDL-chol (mmol/L)	3.06 ± 0.82	2.93 ± 0.75	2.97 ± 0.80	3.03 ± 0.84	2.69 ± 0.68	2.82 ± 0.58	2.73 ± 0.67	2.79 ± 0.60
HDL-chol (mmol/L)	1.59 ± 0.48	1.56 ± 0.36	1.53 ± 0.47	1.43 ± 0.48	1.47 ± 0.04	1.55 ± 0.34	1.52 ± 0.34	1.45 ± 0.35
Triglycerides (mmol/L)	1.54 ± 0.65	1.83 ± 0.76	1.86 ± 0.80	1.85 ± 0.48	1.16 ± 0.58	0.92 ± 0.35	0.97 ± 0.36	1.02 ± 0.49
WBC (10^9/L)	11.7 ± 6.4	10.9 ± 3.1	9.66 ± 2.68	11.2 ± 4.7	5.5 ± 0.1	5.7 ± 1.8	5.81 ± 1.78	5.8 ± 1.9
RBC (10^{12}/L)	4.28 ± 0.05	4.32 ± 0.35	4.37 ± 0.44	4.35 ± 0.44	4.15 ± 0.04	4.17 ± 0.61	4.26 ± 0.67	4.15 ± 0.56
Platelets (10^9/L)	271 ± 10	302 ± 69	306 ± 54	312 ± 79	203 ± 40	214 ± 44	216 ± 48	225 ± 50
Hematocrit (%)	0.380 ± 0.004	0.384 ± 0.040	0.392 ± 0.052	0.391 ± 0.047	0.373 ± 0.004	0.378 ± 0.060	0.386 ± 0.063	0.376 ± 0.058
MMP3 (ng/ml)	245 ± 122	232 ± 84.1	217 ± 93.5	221 ± 112	n.d.	n.d.	n.d.	n.d.
IgG (mg/dl)	1211 ± 357	1244 ± 305	1202 ± 340	1282 ± 353	n.d.	n.d.	n.d.	n.d.

Values represent mean ± SD. n.d., not determined. *$p < 0.05$ by two-way repeated measures ANOVA.

mitochondrial inner membranes and increases production of reactive oxygen species (ROS), which further damages mETS [13,14]. Reduction of the L/P ratios in the open-label and double-blind studies suggests that hydrogen alleviates mETS dysfunction in MM either by scavenging ROS or by yet unidentified signaling mechanisms.

MMP3 belongs to a family of calcium-dependent zinc proteinases induced by cytokines and secreted by inflammatory cells. MMPs enhance T-cell migration and adhesion, and also degrade the extracellular matrix proteins [15]. MMP3 is increased in a fraction of DM patients [16]. MMP3 may facilitate lymphocyte adhesion and enhance T-cell-mediated cytotoxicity by degrading extracellular matrix proteins in DM. Hydrogen improved serum MMP3 levels in the open-label and double-blind studies, which is expected to ameliorate pathogenic inflammatory processes that culminates in muscle fiber destruction.

We observed less prominent effects with the double-blind study compared to the open-label study. The lack of statistically significance in the double-blind study is possibly due to a lower amount of HEW (1.0 vs. 0.5 liter per day) and to a shorter observation period (12 vs. 8 weeks). In the open-label study, drinking 1.0 liter of HEW was not readily accommodated by most myopathic patients. Hydrogen does not show simple dose-response relationship in rodents [2-4], and *ad libitum* administration of even 5%-saturated HEW markedly attenuates development of Parkinson's disease in mice [17]. We thus reduced the amount of hydrogen to 0.5 liter in the double-blind trial, and also shortened the observation period to minimize the burden on the participants. This, however, might have masked effects of HEW. Indeed, when we compare studies of diabetes mellitus type 2 [6], the current open-label trial, and metabolic syndrome [9], the participants took 0.9, 1.0, and 1.5-2.0 liters of HEW, respectively. Ratios of total cholesterol/HDL-cholesterol are available at 8 weeks in all the studies, and are changed to 103.8%, 98.6%, and 95.8%, respectively, of those before hydrogen administration, which is in accordance with a dose-response effect of HEW. Additionally, among the two previous studies [6,9] and the current open-label and double-blind studies, the most prominent effects are observed with 1.5-2.0 liters of HEW. As drinking a large amount of HEW is not easily accommodated by most patients especially in winter, a threshold effect and/or a dose-response effect should be further elaborated for each pathological state.

Conclusions

HEW is effective for mitochondrial dysfunction in MM and inflammatory processes in DM. Hydrogen may have

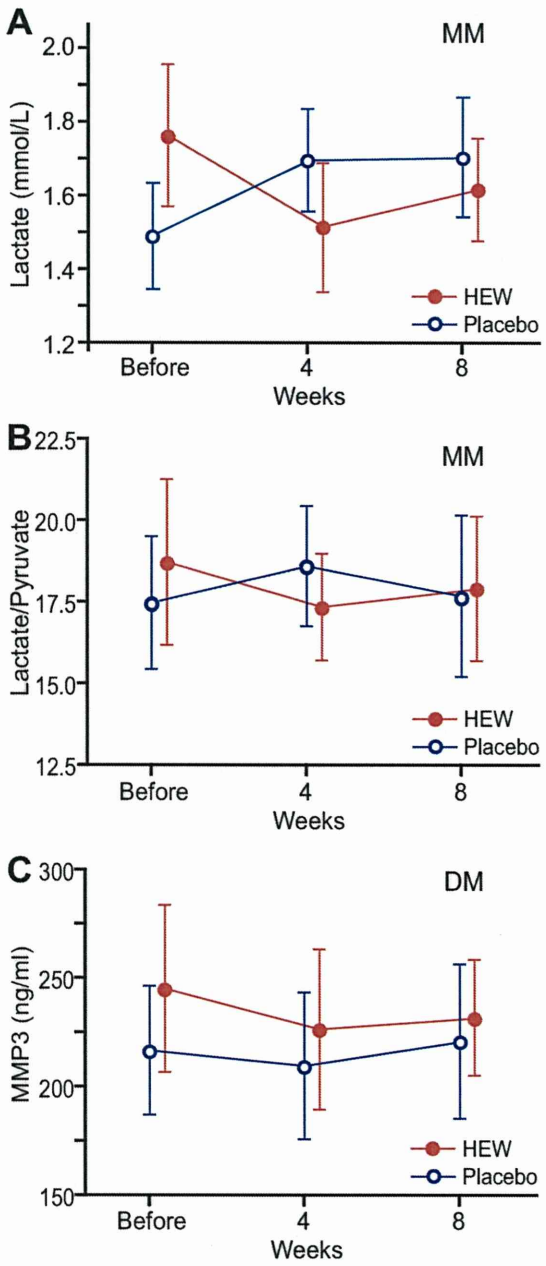

Figure 2 Temporal profiles of three parameters in the double-blind trial. Serum lactate **(A)** and L/P ratios **(B)** in 12 mitochondrial myopathies (MM) patients. **(C)** Serum MMP3 in 10 dermatomyositis (DM) patients. Patients took HEW or placebo for 8 weeks. Means and SD are plotted. **(A)** Serum lactate levels in MM are statistically different by two-way repeated measures ANOVA ($p < 0.05$, Table 1), but the Bonferroni's multiple comparison test reveals no statistical difference between any two values. No statistical difference was observed in L/P ratios **(B)** and serum MMP3 **(C)**. The normal range of lactate is 0.5-2.2 mmol/l. Normal ranges of the other parameters are indicated in Figure 1.

a threshold effect or a dose-response effect and 1.0 liter or more per day of HEW is likely to be required to exert beneficial effects.

Abbreviations

HEW: hydrogen-enriched water; PMD: progressive muscular dystrophy; PM: polymyositis; DM: dermatomyositis; MM: mitochondrial myopathies; CPEO: chronic progressive external ophthalmoplegia; MELAS: mitochondrial myopathy with lactic acidosis and stroke-like episodes; MMP3: matrix metalloproteinase-3.

Acknowledgements

We would like to thank the patients for their participation in these studies. We thank Fumiko Ozawa for her technical assistance. This work was supported by Grants-in-Aid from the Ministry of Health, Labor, and Welfare of Japan and the Ministry of Education, Culture, Sports, Science, and Technology of Japan.

Author details

[1]Division of Neurogenetics, Center for Neurological Diseases and Cancer, Nagoya University Graduate School of Medicine, 65 Tsurumai, Showa-ku, Nagoya 466-8550, Japan. [2]Faculty of Pathophysiology and Therapeutics, Aichi Medical University College of Nursing, 21 Karimata Yazako, Nagakute-cho, Aichi-gun, Aichi 480-1195, Japan. [3]Department of Neurology, Aichi Medical University School of Medicine, 21 Karimata Yazako, Nagakute-cho, Aichi-gun, Aichi 480-1195, Japan. [4]Department of Biomedical Sciences, College of Life and Health Sciences, Chubu University, 1200 Matsumoto, Kasugai, Aichi 487-8501, Japan. [5]Department of Longevity and Aging Research, Gifu International Institute of Biotechnology, 1-1 Nakafudogaoka, Kakamigahara, Gifu 504-0838, Japan.

Authors' contributions

TI and KS examined patients and acquired data. MI[1] and TI organized data and performed statistical analysis. MI[1] and KO wrote the paper. MI[4], MI[5], and KO conceived the study. All authors read and approved the final manuscript.

Competing interests

The authors declare that they have no competing interests.

Received: 24 June 2011 Accepted: 3 October 2011
Published: 3 October 2011

References

1. Ohsawa I, Ishikawa M, Takahashi K, Watanabe M, Nishimaki K, Yamagata K, Katsura K, Katayama Y, Asoh S, Ohta S: **Hydrogen acts as a therapeutic antioxidant by selectively reducing cytotoxic oxygen radicals.** *Nat Med* 2007, **13**:688-694.
2. Ohta S, Nakao A, Ohno K: **The 2011 Medical Molecular Hydrogen Symposium: An Inaugural Symposium of the Journal Medical Gas Research.** *Med Gas Res* 2011, **1**:10.
3. Nakao A, Sugimoto R, Billiar TR, McCurry KR: **Therapeutic Antioxidant Medical Gas.** *J Clin Biochem Nutr* 2009, **44**:1-13.
4. Hong Y, Chen S, Zhang JM: **Hydrogen as a selective antioxidant: a review of clinical and experimental studies.** *J Int Med Res* 2010, **38**:1893-1903.
5. Itoh T, Fujita Y, Ito M, Masuda A, Ohno K, Ichihara M, Kojima T, Nozawa Y, Ito M: **Molecular hydrogen suppresses FcepsilonRI-mediated signal transduction and prevents degranulation of mast cells.** *Biochem Biophys Res Commun* 2009, **389**:651-656.
6. Kajiyama S, Hasegawa G, Asano M, Hosoda H, Fukui M, Nakamura N, Kitawaki J, Imai S, Nakano K, Ohta M, Adachi T, Obayashi H, Yoshikawa T: **Supplementation of hydrogen-rich water improves lipid and glucose metabolism in patients with type 2 diabetes or impaired glucose tolerance.** *Nutr Res* 2008, **28**:137-143.
7. Nakayama M, Kabayama S, Nakano H, Zhu WJ, Terawaki H, Nakayama K, Katoh K, Satoh T, Ito S: **Biological Effects of Electrolyzed Water in Hemodialysis.** *Nephron Clin Pract* 2009, **112**:C9-C15.
8. Nakayama M, Nakano H, Hamada H, Itami N, Nakazawa R, Ito S: **A novel bioactive haemodialysis system using dissolved dihydrogen (H-2)**

produced by water electrolysis: a clinical trial. *Nephrol Dial Transplant* 2010, **25**:3026-3033.
9. Nakao A, Toyoda Y, Sharma P, Evans M, Guthrie N: **Effectiveness of Hydrogen Rich Water on Antioxidant Status of Subjects with Potential Metabolic Syndrome-An Open Label Pilot Study.** *J Clin Biochem Nutr* 2010, **46**:140-149.
10. Kang K-M, Kang Y-N, Choi I-B, Gu Y, Kawamura T, Toyoda Y, Nakao A: **Effects of drinking hydrogen-rich water on the quality of life of patients treated with radiotherapy for liver tumors.** *Med Gas Res* 2011, **1**:11.
11. Ono H, Nishijima Y, Adachi1 N, Tachibana S, Chitoku S, Mukaihara S, Sakamoto M, Kudo Y, Nakazawa J, Kaneko K, Nawashiro H: **Improved brain MRI indices in the acute brain stem infarct sites treated with hydroxyl radical scavengers, Edaravone and hydrogen, as compared to Edaravone alone. A non-controlled study.** *Med Gas Res* 2011, **1**:12.
12. DiMauro S: **Pathogenesis and treatment of mitochondrial myopathies: recent advances.** *Acta Myologica* 2010, **29**:333-338.
13. Wei YH, Lu CY, Wei CY, Ma YS, Lee HC: **Oxidative stress in human aging and mitochondrial disease-consequences of defective mitochondrial respiration and impaired antioxidant enzyme system.** *Chin J Physiol* 2001, **44**:1-11.
14. McKenzie M, Liolitsa D, Hanna MG: **Mitochondrial disease: mutations and mechanisms.** *Neurochem Res* 2004, **29**:589-600.
15. Sternlicht MD, Werb Z: **How matrix metalloproteinases regulate cell behavior.** *Annu Rev Cell Dev Biol* 2001, **17**:463-516.
16. Nishijima C, Hayakawa I, Matsushita T, Komura K, Hasegawa M, Takehara K, Sato S: **Autoantibody against matrix metalloproteinase-3 in patients with systemic sclerosis.** *Clin Exp Immunol* 2004, **138**:357-363.
17. Fujita K, Seike T, Yutsudo N, Ohno M, Yamada H, Yamaguchi H, Sakumi K, Yamakawa Y, Kido MA, Takaki A, Katafuchi T, Nakabeppu Y, Noda M: **Hydrogen in drinking water reduces dopaminergic neuronal loss in the 1-methyl-4-phenyl-1,2,3,6-tetrahydropyridine mouse model of Parkinson's disease.** *PLoS One* 2009, **4**:e7247.

doi:10.1186/2045-9912-1-24
Cite this article as: Ito *et al.*: Open-label trial and randomized, double-blind, placebo-controlled, crossover trial of hydrogen-enriched water for mitochondrial and inflammatory myopathies. *Medical Gas Research* 2011 **1**:24.

Hum Genet (2011) 130:671–683
DOI 10.1007/s00439-011-1006-9

ORIGINAL INVESTIGATION

Hyperuricemia cosegregating with osteogenesis imperfecta is associated with a mutation in *GPATCH8*

Hiroshi Kaneko · Hiroshi Kitoh · Tohru Matsuura · Akio Masuda · Mikako Ito · Monica Mottes · Frank Rauch · Naoki Ishiguro · Kinji Ohno

Received: 28 February 2011 / Accepted: 9 May 2011 / Published online: 19 May 2011

Abstract Autosomal dominant osteogenesis imperfecta (OI) is caused by mutations in *COL1A1* or *COL1A2*. We identified a dominant missense mutation, c.3235G>A in *COL1A1* exon 45 predicting p.G1079S, in a Japanese family with mild OI. As mutations in exon 45 exhibit mild to lethal phenotypes, we tested if disruption of an exonic splicing *cis*-element determines the clinical phenotype, but detected no such mutations. In the Japanese family, juvenile-onset hyperuricemia cosegregated with OI, but not in the previously reported Italian and Canadian families with c.3235G>A. After confirming lack of a founder haplotype in three families, we analyzed *PRPSAP1* and *PRPSAP2* as candidate genes for hyperuricemia on chr 17 where *COL1A1* is located, but found no mutation. We next resequenced the whole exomes of two siblings in the Japanese family and identified variable numbers of previously reported hyperuricemia-associated SNPs in *ABCG2* and *SLC22A12*. The same SNPs, however, were also detected in normouricemic individuals in three families. We then identified two missense SNVs in *ZPBP2* and *GPATCH8* on chromosome 17 that cosegregated with hyperuricemia in the Japanese family. *ZPBP2* p.T69I was at the non-conserved region and was predicted to be benign by *in silico* analysis, whereas *GPATCH8* p.A979P was at a highly conserved region and was predicted to be deleterious, which made p.A979P a conceivable candidate for juvenile-onset hyperuricemia. *GPATCH8* is only 5.8 Mbp distant from *COL1A1* and encodes a protein harboring an RNA-processing domain and a zinc finger domain, but the molecular functions have not been elucidated to date.

Electronic supplementary material The online version of this article (doi:10.1007/s00439-011-1006-9) contains supplementary material, which is available to authorized users.

H. Kaneko · T. Matsuura · A. Masuda · M. Ito · K. Ohno (✉)
Division of Neurogenetics, Center for Neurological Diseases and Cancer, Nagoya University Graduate School of Medicine, 65 Tsurumai, Showa-ku, Nagoya 466-8550, Japan
e-mail: ohnok@med.nagoya-u.ac.jp

H. Kaneko · H. Kitoh · N. Ishiguro
Department of Orthopaedic Surgery, Nagoya University Graduate School of Medicine, Nagoya, Japan

M. Mottes
Department of Life and Reproduction Sciences, University of Verona, Verona, Italy

F. Rauch
Genetics Unit, Shriners Hospital for Children and McGill University, Montreal, QC, Canada

Introduction

Osteogenesis imperfecta (OI) is a heritable connective tissue disorder characterized by bone fragility and low bone mass. Clinical severities are widely variable ranging from intrauterine fractures and perinatal lethality to very mild forms without fractures. Patients also exhibit associated features including blue sclera, dentinogenesis imperfecta, hyperlaxity of ligaments and skin, and hearing loss (Rauch and Glorieux 2004). The widely used classification initially described by Sillence et al. (1979) distinguishes types I, II, III and IV (MIM# 166200, 166210, 259420, and 166220, respectively) on the basis of clinical and radiographic findings. Recently, five additional types of V, VI, VII, VIII and IX (MIM# 610967, 610968, 610682, 610915, and 259440, respectively) have been reported (Cabral et al. 2007; Glorieux et al. 2000, 2002; van Dijk et al. 2009; Ward et al. 2002). OI type I is the mildest form characterized by fractures with little or no limb deformity and

normal or mildly short stature, whereas type II is a perinatal lethal form, mostly due to respiratory failure resulting from multiple rib fractures. Type III is characterized by progressive deformities and fractures that are often present at birth. Severities of types IV, V, VI and VII are between those of types I and III. Type VIII and IX carry features of both types II and III.

Type I collagen is the most abundant bone protein. Most patients (>90%) with OI types I–IV have dominant or recessive mutation(s) in either of two genes, *COL1A1* (MIM# 120150) on chromosome (chr) 17q21.31–q22 and *COL1A2* (MIM# 120160) on chr 7q22.1 that encode the α1 and α2 chains of type I procollagen, respectively (Rauch and Glorieux 2004). A genetic cause of type V remains undetermined to date. Types VI to IX are caused by recessive mutations. Type VI is caused by mutations in *FKBP10* (MIM# 607063) encoding FK506-binding protein 65 (FKBP65) that is a chaperone in type I procollagen folding (Alanay et al. 2010). Type VII is caused by mutations in *CRTAP* (MIM# 605497) encoding cartilage-associated protein (CRTAP) (Morello et al. 2006). Type VIII is caused by mutations in *LEPRE1* (MIM# 610339) encoding prolyl 3-hydroxylase 1 (P3H1) (Cabral et al. 2007). Type IX is caused by mutations in *PPIB* (MIM# 123841) encoding cyclophilin B (CYPB) (van Dijk et al. 2009). CRTAP, P3H1 and CYPB form an intracellular collagen-modifying complex that 3-hydroxylates proline at position 986 in the α1 chain of type I collagen, which is essential for correct folding and stability of the collagen triple helix. Mutations in *CRTAP* and *LEPRE1* are also identified in severe OI phenotypes including type II (Baldridge et al. 2008; Morello et al. 2006). Recently, recessive mutations in *SERPINH1* (MIM# 600943) encoding a chaperone-like protein for collagens, heat shock protein 47 and in *SP7/Osterix* (MIM# 606633) encoding an osteoblast-specific transcription factor have been identified in patients with types III and IV, respectively (Christiansen et al. 2010; Lapunzina et al. 2010).

Two copies of the α1 chain and one copy of the α2 chain form a core triple helix comprising 338 uninterrupted Gly-X–Y triplet repeats, where X is often proline and Y is often hydroxyproline. Gly repeats at every third position are essential for the stability of collagen because larger amino acids cannot be accommodated in the tightly packed core without disruption of the triple helix (Bodian et al. 2008). The most common mutations (>80%) affect one of the repeated Gly residues in the triple helix. More than 800 mutations in *COL1A1* and *COL1A2* are currently deposited in the human type I collagen mutation database (http://www.le.ac.uk/genetics/collagen/) (Dalgleish 1997; Marini et al. 2007). Clinical phenotypes may be determined by the chain in which the Gly substitution occurs, the position of the mutation within the chain and/or the nature of the mutant amino acids (Bodian et al. 2008; Marini et al. 2007; Rauch and Glorieux 2004), but we still cannot predict a clinical phenotype of a given mutation. On the other hand, mutations that create a premature stop codon within *COL1A1* mostly exhibit a milder OI type I. This is because a truncation mutation is unlikely to have a dominant negative effect, but the abundance of type I collagen chain is half of the normal (Marini et al. 2007; Rauch and Glorieux 2004).

Pre-mRNA splicing is regulated by intronic and exonic splicing *cis*-elements. Both constitutively and alternatively spliced exons harbor exonic splicing enhancers (ESEs) and silencers (ESSs). Splicing *trans*-factors are expressed in a developmental stage-specific and tissue-specific manner, and their expressions tightly regulate alternative splicing of an exon carrying ESEs/ESSs. A mutation in the coding region is predicted to exert its pathogenicity by compromising a functional amino acid, but nonsense, missense and even silent mutations potentially disrupt an ESE/ESS, thereby resulting in aberrant splicing (Cartegni et al. 2002, 2003). Indeed, more than 16–20% of exonic mutations are predicted to disrupt an ESE (Gorlov et al. 2003).

Exome resequencing is a powerful and efficient method to identify a novel gene associated with a rare monogenic disorder, especially when the number of unrelated patients or the number of family members of a patient are too small to apply linkage studies. Filtering against existing SNP database and the exomes of unaffected individuals can remove common variants to identify a causal gene. Ng et al. (2009) sequenced exomes of 12 humans, including four unrelated individuals with autosomal dominant Freeman-Sheldon syndrome (MIM# 193700) and eight HapMap individuals. They successfully identified mutations in *MYH3* (MIM# 160720) in all the affected individuals. Ng et al. (2010b) also sequenced exomes of four patients in three families with autosomal recessive Miller syndrome (MIM# 263750) and de novo identified compound heterozygous mutations in *DHODH* (MIM# 126064). Ng et al. (2010a) additionally sequenced exomes of ten unrelated patients with autosomal dominant Kabuki syndrome (MIM# 147920) and de novo identified nonsense or frameshift mutations in *MLL2* (MIM# 602113). Similarly, Lalonde et al. (2010) sequenced two unrelated fetuses with autosomal recessive Fowler syndrome (MIM# 225790) and de novo identified compound heterozygous mutations in *FLVCR2* (MIM# 610865).

In a Japanese family with OI type I, hyperuricemia cosegregated with OI. To our knowledge, association of hyperuricemia with OI has been reported in two families, in which two of three OI patients had gouty arthritis and hyperuricemia at young ages (Allen et al. 1955). Underexcretion of urate is causally associated with mutations in *UMOD* (MIM# 191845) encoding uromodulin (Hart et al.

2002) as well as with SNPs in three genes: *SLC2A9* (MIM# 606142) encoding glucose transporter 9 (Doring et al. 2008; Vitart et al. 2008), *ABCG2* (MIM# 603756) encoding ATP-binding cassette subfamily G member 2, a urate transporter (Dehghan et al. 2008; Kolz et al. 2009; Stark et al. 2009; Woodward et al. 2009), and *SLC22A12* (MIM# 607096) encoding URAT1, a renal urate-anion exchanger (Graessler et al. 2006; Tabara et al. 2010). On the other hand, overproduction of urate is caused by mutations in *PRPS1* (MIM# 311850) encoding PRPP synthetase I (Roessler et al. 1993) and *HPRT1* (MIM# 308000) encoding hypoxanthine guanine phosphoribosyltransferase 1 (Gibbs and Caskey 1987).

We here identified a dominant missense mutation, c.3235G>A in *COL1A1* exon 45 predicting p.G1079S, in a Japanese family with OI type I and hyperuricemia, and analyzed the molecular bases of two clinical features. First, we tested if mild to lethal phenotypes of mutations in exon 45 of *COL1A1* were accounted for by preservation or disruption of an ESE/ESS element, and found that ESE/ESS elements were not involved in disease severities. Second, we traced a cause of the hyperuricemia by exome resequencing of two siblings and found that a missense mutation in *GPATCH8* encoding the G patch domain-containing protein 8 close to *COL1A1* cosegregated with hyperuricemia.

Patients and methods

Samples and ethical considerations

We obtained blood from each family member and isolated genomic DNA (gDNA) from 2 ml of peripheral blood using the QIAamp DNA Blood Midi Kit (Qiagen) according to the manufacturer's instructions. We also obtained skin biopsy of an affected individual (II-3) of a Japanese family (F1) and cultured non-transformed fibroblasts for splicing and sequencing analysis. Informed consent was obtained from all family members. The studies have been approved by the Institutional Review Boards of the Nagoya University, the University of Verona and the McGill University. Clinical features and mutational analyses have been previously reported in the Italian and Canadian families (Mottes et al. 1992; Roschger et al. 2008).

Microsatellite analysis of *COL1A1* and *COL1A2* to identify a mutation in the Japanese family

We genotyped all family members for three microsatellite markers flanking *COL1A1* (D17S1293, −16 Mbp; D17S1319, −14 kbp; and D17S788, 2 Mbp). As no annotated microsatellite markers were available close to *COL1A2*, we posted three new microsatellite markers to DDBJ (AB499843, −17 kbp; AB499844, 29 kbp; and AB499845, 123 kbp) and analyzed them in the family. We fluorescently labeled the 5′ end of each forward primer with 5FAM (Sigma-Aldrich), and amplified microsatellite markers with the HotStarTaq Plus Master Mix (Qiagen) using gDNA and primers indicated in Supplementary Table 1.

We mixed 1.5 μl of 20-times diluted PCR product with 0.5 μl of GeneScan-500 ROX Size Standard (Applied Biosystems) and 24.5 μl of formamide, and incubated the mixture at 95°C for 3 min. The mixture was run by capillary electrophoresis on an ABI PRISM 310 Genetic Analyzer and was analyzed with the GeneScan and GeneMapper software (Applied Biosystems).

Sequence analysis of *COL1A1*

After the microsatellite analysis suggested that *COL1A1* was more likely to be a causative gene, we amplified all exons and flanking intronic regions of ~40 bp, as well as 5′ and 3′ UTRs of *COL1A1* from gDNA of II-3 by PCR. We performed the dye terminator cycle sequencing reaction with the GenomeLab DTCS Quick Start Kit (Beckman Coulter) and ran on the CEQ 8000 Genetic Analysis System (Beckman Coulter) according to the manufacturer's instructions. We compared the chromatograms with the GenBank reference sequences of *COL1A1* gDNA using the Mutation Surveyor software version 2.61 (SoftGenetics). We numbered *COL1A1* mutations with the translation initiator methionine as amino acid +1, and the A of the ATG codon as nucleotide +1 according to the Human Genome Variation Society (http://www.hgvs.org/mutnomen/recs.html). We numbered exons according to the human type I collagen mutation database (http://www.le.ac.uk/genetics/collagen/), in which *COL1A1* exon 33 is named *COL1A1* exon 33–34 to match the exonic annotations of *COL1A2*.

Allele-specific primer (ASP)-PCR to trace the *COL1A1* mutation

We traced the mutation in family members using ASP-PCR. The wild-type ASP was 5′-TCCCGCCGGTCCT GTAGG-3′, and the mutant ASP was 5′-TCCCGCCGG TCCTGTAAG-3′, where the mutated nucleotide is underlined, and an artificially introduced mismatch is shown in bold. The reverse primer was 5′-GCCACGGTGAC CCTTTATGC-3′.

Prediction of effects of mutations on pre-mRNA splicing

Five missense mutations in exon 45 of *COL1A1* cause mild to lethal OI phenotypes (Fig. 2a) (Constantinou et al. 1989;

Hartikka et al. 2004; Lund et al. 1997; Marini et al. 2007; Mottes et al. 1992; Roschger et al. 2008). We predicted the effects on pre-mRNA splicing of 18 sequence variants with or without each mutation in the presence or absence of each of two SNPs (rs1800215 and rs1800217) in exon 45 of *COL1A1* (Fig. 2b) using five Web-based programs: ESEfinder 3.0 (http://rulai.cshl.edu/cgi-bin/tools/ESE3/esefinder.cgi?process=home) (Cartegni et al. 2003), ESR-search (http://ast.bioinfo.tau.ac.il/) (Goren et al. 2006), FAS-ESS (http://genes.mit.edu/fas-ess/) (Wang et al. 2004), PESXs (http://cubweb.biology.columbia.edu/pesx/) (Zhang and Chasin 2004; Zhang et al. 2005), and RESCUE-ESE (http://genes.mit.edu/burgelab/rescue-ese/) (Fairbrother et al. 2002). We also predicted the effects of the mutations on splice site strength of the 18 sequence variants using two Web-based programs: the NetGene2 Server (http://www.cbs.dtu.dk/services/NetGene2/) (Brunak et al. 1991; Hebsgaard et al. 1996) and the Splice Site Prediction by Neural Network (http://www.fruitfly.org/seq_tools/splice.html) (Reese et al. 1997).

Splicing analysis of fibroblasts of the OI patient (II-3)

We first examined splicing of *COL1A1* exon 45 in the patient's fibroblasts. We extracted total RNA from cultured fibroblasts of II-3 using Trizol reagent (Invitrogen) and synthesized cDNA using the oligo(dT)$_{12-18}$ primer (Invitrogen) and the ReverTra Ace reverse transcriptase (Toyobo). We examined skipping of *COL1A1* exon 45 using 5′-GGTTCCCCTGGACGAGAC-3′ on exon 43 and 5′-TCCAGAGGGACCTTGTTCAC-3′ on exon 47. We also sequenced RT-PCR products as described above to scrutinize splicing consequences. As skipping of exon 45 results in an in-frame deletion of 54 nucleotides, we did not downregulate the nonsense-mediated mRNA decay (NMD) before harvesting cells.

COL1A1 minigene constructs

We amplified exons 44–46 and the intervening introns of *COL1A1* (Fig. 2b) by PCR. The PCR primers introduced a *Hin*dIII site and the Kozak consensus sequence of 5′-CCACCATG-3′ to the 5′ end, as well as a TAA stop codon and a *Bam*HI site at the 3′ end of the PCR product, so that the minigene transcript is tolerant to NMD (Ohno et al. 2003). We inserted the PCR product into the pcDNA3.1(+) mammalian expression vector (Invitrogen) and confirmed the lack of PCR artifacts by sequencing the entire insert. We next constructed 17 variant minigenes using the QuikChange site-directed mutagenesis kit (Stratagene) (Fig. 2b). We again confirmed presence of the introduced mutations and absence of artifacts by sequencing the entire inserts.

Splicing assays of *COL1A1* exon 45

We transfected 500 ng of a minigene construct into 50% confluent HEK293 cells in a 12-well plate using the FuGENE 6 transfection reagent (Roche Applied Science) according to the manufacturer's instructions. After 48 h, we extracted total RNA from HEK293 cells and synthesized cDNA as described above. To prevent amplification of the endogenous *COL1A1*, we used generic primers of 5′-TTAATACGACTCACTATAGGGAGACC-3′ and 5′-TTAAGGAGGGCCAGGGGG-3′ located on pcDNA3.1. Untransfected cells were used as a negative control.

Founder analysis of three families with *COL1A1* c.3235G>A

To examine if the *COL1A1* c.3235G>A mutation arose from a common founder in the Japanese, Italian (Mottes et al. 1992) and Canadian (Roschger et al. 2008) families, we genotyped three microsatellite markers flanking *COL1A1* described above and sequenced an intragenic SNP (rs2075554) of *COL1A1* in the Italian and Canadian families (Fig. 1).

Sequence analysis of *PRPSAP1* and *PRPSAP2*

To seek for a responsible gene for hyperuricemia, we sequenced the entire coding regions of *PRPSAP1* and *PRPSAP2* on chr 17 using cDNA synthesized from cultured fibroblasts of II-3.

Resequencing of exome-enriched DNA

As we found no mutation in *PRPSAP1* and *PRPSAP2*, we enriched exonic regions of genomic DNA of II-2, II-3 and VIII-2 using the SureSelect human all exon kit v1 (Agilent Technologies) that covers 1.22% (34 Mbp) of the human genome. We sequenced 50 base pairs of each tag in a single direction using a quarter of a cell of the SOLiD 3 Plus system (Life Technologies) for each sample.

For II-2, II-3 and VIII-2, we obtained 79.1, 68.6 and 109.9 $\times$ 10^6 tags of 50-bp SOLiD reads and mapped 2.18 (69.6%), 1.87 (68.5%) and 3.37 (76.5%) Gbp to the human genome hg19/GRCh37, which yielded a mean coverage of 64.1, 55.1 and 99.0, respectively. Among the mapped tags, 70.1, 72.0 and 73.1% were located on the SureSelect exome probes. Among the 34-Mbp regions where the exome probes were designed, 3.4, 3.6 and 3.5% of nucleotides

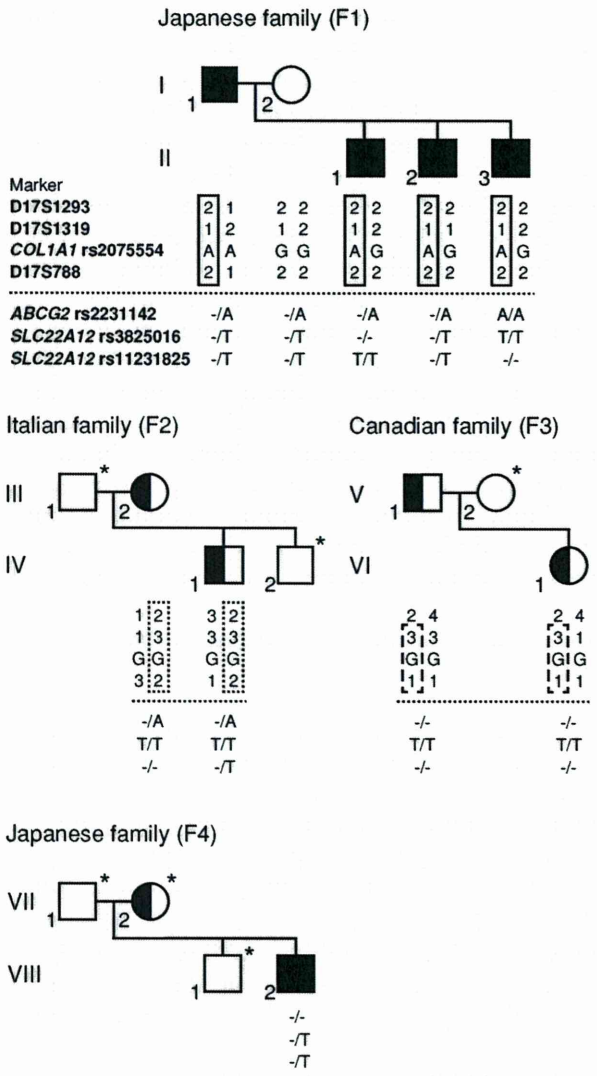

Fig. 1 Pedigrees, haplotypes and genotypes of the Japanese (F1 and F4), Italian (F2) and Canadian (F3) families. Patients in F1, F2 and F3 have c.3235G>A predicting p.G1079S in *COL1A1*. A patient in F4 has c.577G>T predicting p.G193C in *COL1A2*. *Closed symbols* indicate patients with OI and with hyperuricemia. *Half-shaded symbols* represent OI without hyperuricemia. *Asterisks* indicate that DNA sample is not available for our studies. Clinical subtypes are all type I except for the Canadian father (V-1), who exhibits type IV. In F1, hyperuricemia cosegregates with OI. Genotypes of three microsatellite markers (D17S1293, −16 Mbp; D17S1319, −14 kbp; and D17S788, 2 Mbp) flanking *COL1A1* and an SNP (rs2075554) in intron 11 of *COL1A1* are indicated for all the available members in F1, F2, and F3. F1, F2 and F3 carry their unique haplotypes (shown by *solid*, *dotted* and *broken boxes*, respectively). The D17S1293 genotype in F3 is not informative and is not boxed. Genotypes of hyperuricemia-associated SNPs (rs2231142, rs3825016 and rs11231825) are indicated at the bottom of each pedigree tree

were not sequenced at all. Search for single nucleotide variants (SNVs) and indels with Bioscope 1.2.1 (Life Technologies) detected 52,436, 56,941 and 60,303 SNVs/indels. SNVs and indels were compared to dbSNP Build 132.

Analysis of variants in *KRBA2, ZPBP2* and *GPATCH8*

To trace if variants in *KRBA2*, *ZPBP2* and *GPATCH8* cosegregated with hyperuricemia, we analyzed all family members in the Japanese family (F1) by capillary sequencing.

We traced two variants, *ZPBP2* c.206C>T and *GPATCH8* c.2935G>C, in the Italian and Canadian families and 100 normal human genomes using ASP-PCR. The forward primers of *ZPBP2* and *GPATCH8* were 5′-CGT GTCTTCAGCACAAAATGG-3′ and 5′-AGAAGCCGTA GCACCACTCC-3′, respectively. The reverse primers were 5′-GGCCCAATCCATAAGTACAT-3′ and 5′-CCCA TGATCTCTTCCTGGAG-3′, respectively. The mutated nucleotide is underlined, and an artificially introduced mismatch is shown in bold.

To search for the identified variants in *ZPBP2* and *GPATCH8* in normal controls, we mapped 50 Tibetan exome reads (SRA accession number SRP002446) (Yi et al. 2010) to a 200-bp region spanning c.206C>T in exon 3 of *ZPBP2* and a 200-bp region spanning c.2935G>C in exon 8 of *GPATCH8* with the bowtie alignment tool version 0.12.7 (Langmead et al. 2009) using default parameters.

We analyzed amino acid conservations of *ZPBP2* and *GPATCH8* using the evolutionary annotation database, Evola, at the H-Inv DB (http://www.h-invitational.jp/evola/). We also predicted functional effects of amino acid substitutions using two Web-based programs: PolyPhen-2 (http://genetics.bwh.harvard.edu/pph2/) (Adzhubei et al. 2010) and SIFT (http://sift.jcvi.org/) (Kumar et al. 2009).

Results

Hyperuricemia cosegregated with OI type I in the Japanese family (F1)

In a Japanese family (F1), a father (age 56 years) and his three sons (ages 29, 26 and 23 years) had OI type I with blue sclera, dentinogenesis imperfecta and joint laxity (Fig. 1). Two sons (II-1 and II-3) had histories of more than ten fractures before age 13 years, but the father (I-1) and another son (II-2) experienced no bone fracture. One son (II-1) had hearing loss from age 10 years likely due to fractures or deformities of small bones in the middle ear and had hip joint deformities due to repeated femoral fractures. Interestingly, all the affected members had hyperuricemia of ~8 mg/dl that was diagnosed at ages 15–30 years. One son (II-3) had a gout attack, and the other two (I-1 and II-1) had urinary stones. Hyperuricemia is currently well controlled by medication in all the members.

Heteroallelic c.3235G>A mutation in *COL1A1* in the Japanese family (F1)

Genotypes of three microsatellite markers flanking *COL1A1* cosegregated with the OI phenotype in F1 (Fig. 1), whereas genotypes of three markers flanking *COL1A2* did not (data not shown). We thus sequenced the entire exons and the flanking noncoding regions and identified a heteroallelic c.3235G>A mutation in exon 45 and a heteroallelic G/A SNP (rs2075554) in intron 11 of *COL1A1*. The c.3235G>A mutation predicts p.G1079S. We genotyped c.3235G>A in family members by ASP-PCR, and found that all affected members were heterozygous for c.3235G>A (Fig. 1).

Phenotypic variability of osteogenesis imperfecta is not accounted for by disruption of splicing *cis*-elements

In addition to c.3235G>A, four more mutations and two SNPs have been reported in *COL1A1* exon 45 with variable phenotypes ranging from mild type I to perinatal lethal type II (Fig. 2a) (Constantinou et al. 1989; Hartikka et al. 2004; Lund et al. 1997; Marini et al. 2007; Mottes et al. 1992; Roschger et al. 2008). We thus hypothesized that disruption or de novo generation of a splicing *cis*-element determines the clinical phenotype. The five mutations and two SNPs in *COL1A1* exon 45 were predicted to affect 16 putative splicing *cis*-elements by ESEfinder, ESRsearch and PESXs (Table 1). FAS-ESS and RESCUE-ESE predicted no splicing *cis*-elements. All the five mutations with or without two SNPs in *COL1A1* exon 45 variably but slightly weaken acceptor and/or donor splice site strengths according to the NetGene2 (Table 2). The splice site prediction by neural network also predicted that c.3235G>A generates a weak cryptic splice acceptor site in *COL1A1* exon 45 (Table 2). We first examined cultured fibroblasts of II-3 by RT-PCR and found that the *COL1A1* c.3235G>A mutation did not induce aberrant splicing of *COL1A1* (data not shown). NMD was unlikely to have masked aberrant splicing, because we observed heterozygous peaks at c.3235G>A in sequencing the RT-PCR product. We next constructed 18 *COL1A1* minigenes with or without each of the five mutations in the presence or absence of each of the two SNPs (Fig. 2b). RT-PCR analysis of transfected HEK293 cells showed that all minigene constructs gave rise to a single fragment of 336 bp, indicating that splicing was not affected in any mutations or SNPs (Fig. 2c).

Japanese (F1), Italian (F2) and Canadian (F3) families with *COL1A1* c.3235G>A share no founder haplotype

We previously reported *COL1A1* c.3235G>A in the Italian and Canadian families (Marini et al. 2007; Roschger et al. 2008). Although we have not measured serum urate concentrations in these families, gout or urinary stone has not been documented in either family, which suggests that hyperuricemia is not simply due to c.3235G>A.

To pursue if a gene responsible for hyperuricemia is on the same chr as *COL1A1*, we looked for a founder haplotype for c.3235G>A in three families by genotyping three microsatellite markers flanking *COL1A1* (D17S1293, −16 Mbp; D17S1319, −14 kbp; and D17S788, 2 Mbp) and an SNP (rs2075554) in intron 11 of *COL1A1*. The analysis revealed that each family carried a unique haplotype and shared no founder haplotype (Fig. 1). Thus, the mutation is likely to have occurred independently in three ethnic groups. Alternatively, c.3235G>A is an ancient founder mutation, and subsequent multiple recombinations and divergence of microsatellite repeats have obscured a founder effect. In either case, lack of a found haplotype supports the notion that a gene responsible for hyperuricemia is potentially but not necessarily linked to *COL1A1*.

Hyperuricemia is not caused by mutations in *PRPSAP1* or *PRPSAP2*

We thus first looked into candidate genes for hyperuricemia on chr 17 where *COL1A1* (17q21.31–q22) is located. Two candidate genes for hyperuricemia are on chr 17: *PRPSAP1* (MIM# 601249) at 17q24–q25 encoding PAP39 (Ishizuka et al. 1996) and *PRPSAP2* (MIM# 603762) at 17p12-p11.2 encoding PAP41 (Katashima et al. 1998). PAP39 and PAP41 are subunits of phosphoribosylpyrophosphate (PRPP) synthetase that leads to urate production. No mutation has been reported in either gene in any diseases. We sequenced cDNAs of *PRPSAP1* and *PRPSAP2* in II-3, but found no mutation in either gene. As we detected no heterozygous SNPs in *PRPSAP1* and *PRPSAP2*, a mutant allele carrying a premature stop codon might have been missed due to mRNA degradation by NMD.

Resequencing of exomes reveals hyperuricemia-associated SNPs

We next traced a causative gene for hyperuricemia in two siblings (II-2 and II-3) by exome resequencing with the SureSelect human all exon kit v1 (Agilent) and with the SOLiD 3 Plus sequencer (Life Technologies).

We similarly analyzed an unrelated Japanese male (22-year-old) with OI type I and hyperuricemia (VIII-2 in F4 in Fig. 1). His hyperuricemia was by chance detected at age 14 years when he had fractures. His hyperuricemia has been well controlled by medication since then. Exome resequencing of VIII-2 disclosed a novel heteroallelic c.577G>T mutation in *COL1A2* exon 12 predicting

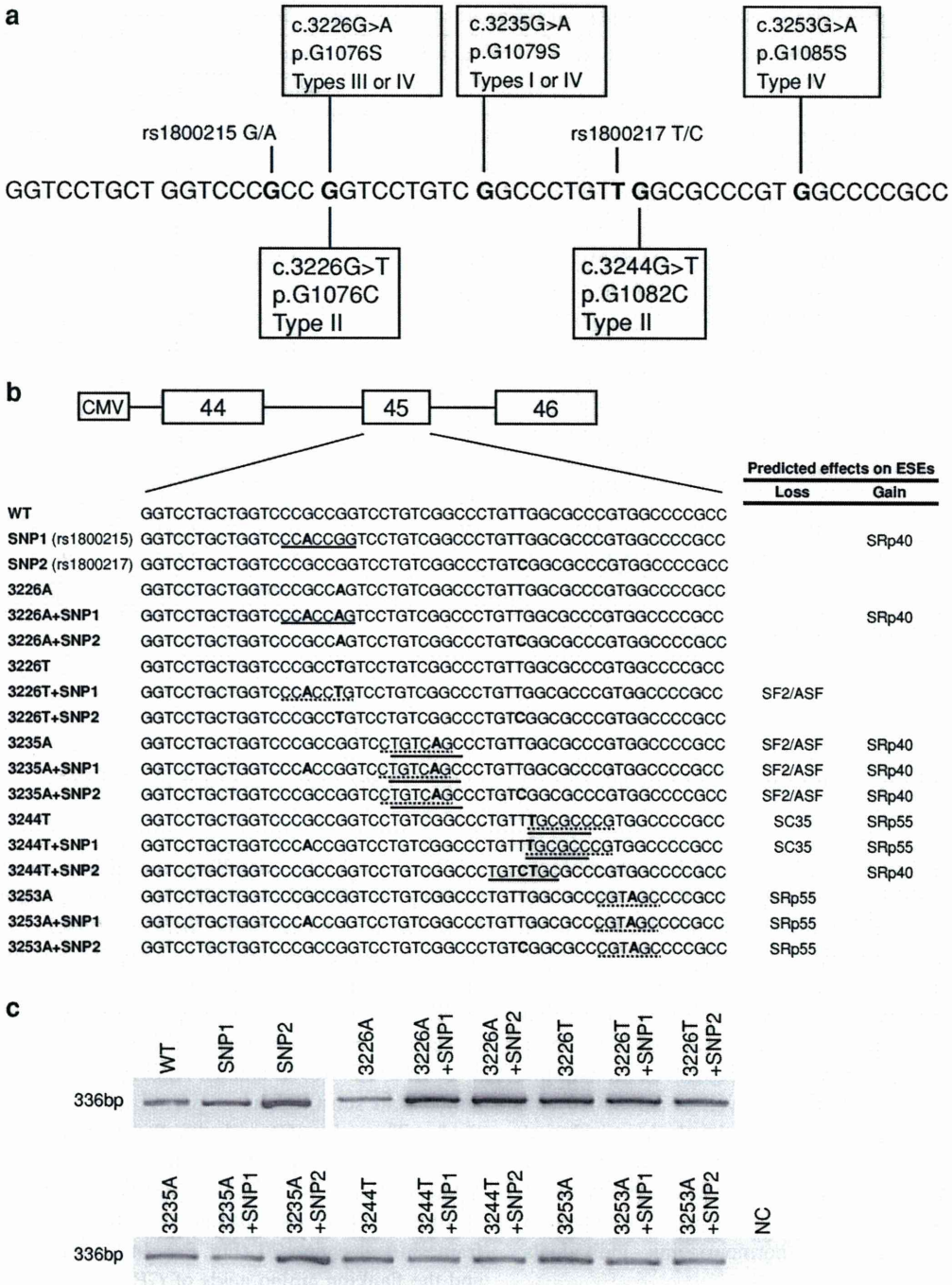

Fig. 2 Splicing assays of *COL1A1* minigenes in HEK293 cells. **a** Positions and phenotypes of OI mutations in *COL1A1* exon 45. Mutations above the wild-type sequence exhibit non-lethal phenotypes, whereas those below the sequence cause a lethal phenotype. **b** Schematic representation of *COL1A1* minigenes. Sequences of mutant minigenes are indicated *below*. Substituted nucleotides are shown in *bold*. Predicted gain and loss of splicing *cis*-elements by ESEfinder (Cartegni et al. 2003) are indicated by *solid* and *dotted underlines*, respectively. **c** RT-PCR of minigenes introduced into HEK293 cells. All constructs show a single fragment of 336 bp, indicating that *COL1A1* exon 45 is not skipped in any constructs. Untransfected cells are used as a negative control (*NC*)

p.G193C. We confirmed the mutation by capillary sequencing. Family samples were not available for our analysis.

In F1, a probability that three siblings inherited an identical allele from the father is $(1/2)^3 = 12.5\%$, which indicates that the causative gene is anywhere in the

Table 1 Affected putative splicing *cis*-elements in *COL1A1* exon 45 predicted by ESEfinder, ESRsearch and PESXs

Sequence variation	Normal allele	Variant allele	Predicted effect	Score[d]		Putative *trans*-factor
				Normal	Variant	
rs1800215	CC**G**CCGG	CC**A**CCGG[a]	Gain	1.622	4.231	SRp40
rs1800217	CTGT**T**GGC	CTGT**C**GGC[c]	Gain		n.a.	
c.3226G>A	CGCC**G**G	CGCC**A**G[b]	Gain		n.a.	
	CC**G**GTCCT	CC**A**GTCCT[c]	Gain		n.a.	
c.3226G>A+rs1800215	CC**G**CC**G**G	CC**A**CC**A**G[a]	Gain	1.622	3.663	SRp40
c.3226G>T	CGCC**G**G	CGCC**T**G[b]	Gain		n.a.	
c.3226G>T+rs1800215	CC**G**CC**G**G	CC**A**CC**T**G[a]	Loss	3.498	0.571	SF2/ASF
c.3235G>A	CTGTC**G**G	CTGTC**A**G[a]	Loss	2.492	0.713	SF2/ASF
	CTGTC**G**GC	CTGTC**A**GC[c]	Loss		n.a.	
	TGTC**G**GC	TGTC**A**GC[a]	Gain	1.058	3.613	SRp40
	GTC**G**GC	GTC**A**GC[b]	Gain		n.a.	
	C**G**GCCCTG	C**A**GCCCTG[c]	Gain		n.a.	
c.3244G>T	**G**GCGCCCG	**T**GCGCCCG[a]	Loss	3.109	1.059	SC35
	GGCGCC	**T**GCGCC[a]	Gain	0.721	3.531	SRp55
c.3244G>T+rs1800217	TGT**TG**GC	TGT**CT**GC[a]	Gain	−1.326	3.367	SRp40
c.3253G>A	CGT**G**GC	CGT**A**GC[a]	Loss	2.940	2.331	SRp55

Variant nucleotides are shown in bold and underlined

n.a. not applicable

[a] ESEfinder

[b] ESRsearch

[c] PESXs

[d] Default threshold values employed by ESEfinder are SRp40 = 2.67, SF2/ASF = 1.867, SC35 = 2.383 and SRp55 = 2.676

12.5% regions of the entire genome. We first sought for a mutation responsible for hyperuricemia in 24 genes (see Table 3 and Suppl. Table 2) that are involved in urate metabolisms and excretion, but found none in either patient. We then scrutinized SNPs in ten genes that are known to be associated with hyperuricemia and identified 12 SNPs (Table 3). In this analysis, we excluded SNPs with a minor allelic frequency of 0.01 or less. Among the 12 SNPs, rs2231142 in *ABCG2* as well as rs3825016 and rs11231825 in *SLC22A12* are previously reported and will be addressed in the discussion. We traced the three SNPs in F1, F2 and F3 by capillary sequencing and found that variable dosages of these SNPs were observed in hyperuricemic as well as in normouricemic individuals (Fig. 1).

A missense mutation in *GPATCH8* is likely to lead to hyperuricemia in the Japanese family (F1)

After eliminating SNPs in the dbSNP132 database, only three non-synonymous variants remained shared between II-2 and II-3 on chr 17; c.602A>G in exon 2 of *KRBA2* at 17p13.1, c.206C>T in exon 3 of *ZPBP2* (MIM# 608499) at 17q12 (Fig. 3a) and c.2935G>C in exon 8 of *GPATCH8* at 17q21.31 (Fig. 3b). Capillary sequencing revealed that variants in *ZPBP2* and *GPATCH8* cosegregated with hyperuricemia in F1, but the *KRBA2* variant did not. These two variants were not detected in F2, F3, F4, 100 normal human individuals or exomes of 50 Tibetans (Yi et al. 2010). In addition, exome-capture resequencing of VIII-2 detected no mutations in *ZPBP2* and *GPATCH8*.

ZPBP2 c.206C>T and *GPATCH8* c.2935G>C predict amino acid substitutions of p.T69I and p.A979P, respectively. Threonine 69 and the flanking amino acids of *ZPBP2* are not conserved across mammalian species. Additionally, an SNP rs35591738 mutates the N-terminal proline at codon 68, and an SNP rs34272593 causes a frameshift at codon 70 (Fig. 3a). In contrast, alanine 979 and the flanking amino acids of *GPATCH8* are in the serine-rich region and are highly conserved across mammalian species (Fig. 3b). PolyPhen-2 (Adzhubei et al. 2010) predicted that *ZPBP2* p.T69I was benign with a score of 0.025 and *GPATCH8* p.A979P was damaging with a score of 0.988, where 1.0 was the worst score. Similarly, SIFT (Kumar et al. 2009) predicted that *ZPBP2* p.T69I was tolerated with a score of 0.38 and *GPATCH8* p.A979P was damaging with a score of 0.00, where a score < 0.05 was predicted to be deleterious.

Table 2 Splice site strength of *COL1A1* exon 45 predicted by the NetGene2 and the Splice Site Prediction by Neural Network

Sequence variation	NetGene2		Splice Site Prediction by Neural Network	
	Confidence		Score	
	Acceptor	Donor	Acceptor	Donor
Wild type	0.97	0.93	0.98	0.95
rs1800215	–	–	–	–
rs1800217	–	–	–	–
c.3226G>A	–	0.89	–	–
c.3226G>A+rs1800215	0.94	0.89	–	–
c.3226G>A+rs1800217	–	0.89	–	–
c.3226G>T	0.94	0.87	–	–
c.3226G>T+rs1800215	0.94	0.86	–	–
c.3226G>T+rs1800217	0.94	0.87	–	–
c.3235G>A	0.94	0.87	–	–
c.3235G>A+rs1800215	0.94	0.86	–	–
c.3235G>A+rs1800217	0.94	0.87	–	–
c.3244G>T	0.94	0.86	–	–
c.3244G>T+rs1800215	0.94	0.86	–	–
c.3244G>T+rs1800217	0.94	0.86	–	–
c.3253G>A	0.94	0.88	0.52[a]	–
c.3253G>A+rs1800215	0.94	0.87	0.52[a]	–
c.3253G>A+rs1800217	–	0.89	–	–

– symbol represents being identical to the wild-type

[a] In addition to the native splice acceptor site of 0.98, a cryptic splice acceptor site 'AG' is generated at c.3253_3254

Table 3 Twelve SNPs identified by exome resequensing in five out of ten genes associated with hyperuricemia

Ch	Gene	Position	Nuc.	Amino acid	AF	dbSNP	II-2	II-3	VIII-2
1	*AGL*	100,336,361	C > T	Syn.	0.7	rs2230306	T/T	–/T	–/T
4	*ABCG2*[b]	89,034,551	G > A	Syn.	0.02	rs35622453	–/–	–/–	–/A
		89,052,323	C > A	Q141K	0.31	rs2231142	–/A	A/A	–/–
		89,061,114	G > A	V12M	0.19	rs2231137	–/A	–/–	–/A
4	*SLC2A9*[b]	9,909,923	C > T	P350L	0.33	rs2280205	–/T	–/T	–/–
		9,922,130	G > A	R294H	0.72	rs3733591	–/A	–/–	–/A
		9,998,440	G > A	Syn.	0.54	rs10939650	–/A	A/A	–/A
		10,022,981	G > A	G25R	0.43	rs2276961	–/A	–/A	–/–
		10,027,542	G > A	A17T	0.06	rs6820230	–/–	–/A	–/A
11	*SLC22A12*[b]	64,359,286	C > T	Syn.	0.21	rs3825016	–/T	T/T	–/T
		64,360,274	C > T	Syn.	0.81	rs11231825	–/T	–/–	–/T
12	*PFKM*		n.d.						
16	*UMOD*[b]		n.d.						
17	*G6PC*		n.d.						
X	*HPRT1*[a]		n.d.						
X	*PRPS1*[a]		n.d.						
X	*MAOA*	43,591,036	G > T	Syn.	0.3	rs6323	–/–	T/T	T/T

[a] The gene is associated with purine metabolism

[b] The gene is associated with renal excretion of urate

– symbol represents in the patients' genotypes mean being identical to the reference nucleotides

Syn synonymous nucleotide change, *AF* allelic frequency of the changed nucleotide, *n.d.* no SNPs are detected

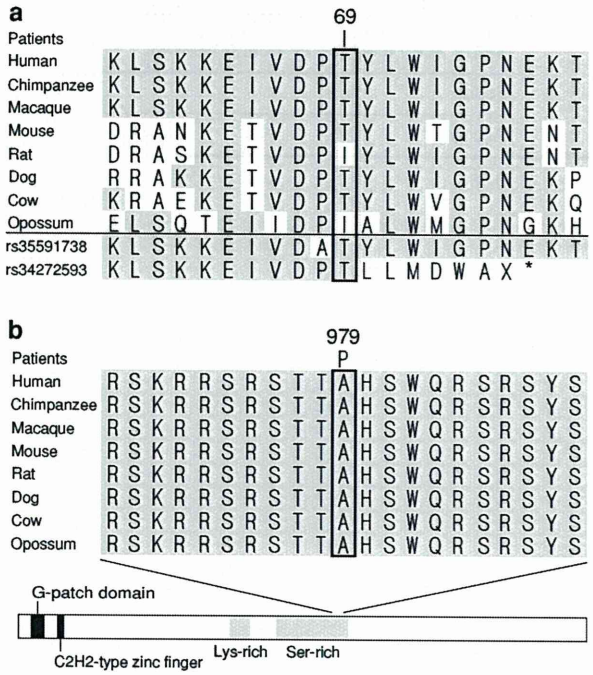

Fig. 3 Conservation of 21 amino acid segments encoded by *ZPBP2* and *GPATCH8* in mammals. Locations of non-synonymous variants identified in the Japanese family (F1) are *boxed*. Amino acids identical to human are *shaded*. **a** c.206C>T predicts p.T69I in *ZPBP2*. T69 is not conserved in rat and opossum. An SNP rs35591738 predicts p.P68A, and an SNP rs34272593 induces a frameshift. **b** c.2935G>C predicts p.A979P in *GPATCH8*. The mutation is located at the C-terminal end of the serine-rich region

Discussion

Phenotypic variabilities of OI mutations

We identified a heteroallelic c.3235G>A mutation in *COL1A1* exon 45 in a Japanese family with mild OI type I. The c.3235G>A mutation has been previously reported in six families with OI types I (Hartikka et al. 2004; Mottes et al. 1992; Roschger et al. 2008) and IV (Marini et al. 2007). *COL1A1* exon 45 encodes six of the 338 Gly-X–Y triplet repeats. Four additional mutations have been reported in exon 45 (Constantinou et al. 1989; Lund et al. 1997; Marini et al. 2007), and all substitute Ser or Cys for Gly (Fig. 2a) with mild to lethal phenotypes. Among the five mutations, two mutations introducing Cys result in a lethal type II, whereas three mutations introducing Ser give rise to milder types I, III and IV. This notion, however, cannot be applied to the other exons according to the human type I collagen mutation database (http://www.le.ac.uk/genetics/collagen/).

Being prompted by a report that more than 16–20% of exonic mutations disrupt an ESE (Gorlov et al. 2003), we asked if a mutation disrupting an ESE in exon 45 causes skipping of an inframe exon 45 and exhibits a severe dominant negative phenotype. Three Web-based programs predict that all the five mutations and the two SNPs affect 16 putative exonic splicing *cis*-elements (Table 1). We thus constructed and analyzed 18 minigenes carrying all possible combinations of the five mutations and two SNPs (Fig. 2b), but found that none affected pre-mRNA splicing (Fig. 2c). Our analysis suggests that the currently available algorithms of splicing *trans*-factors cannot efficiently predict splicing *cis*-elements. This is likely because the recognition motifs of splicing *trans*-factors are mostly determined by in vitro SELEX experiments. A recently developed technique, the high throughput sequencing coupled to crosslinking immunoprecipitation method (HITS-CLIP), enables us to extensively determine RNA segments recognized by a specific splicing *trans*-factor in vivo (Licatalosi et al. 2008; Yeo et al. 2009). Accumulation of knowledge with the HITS-CLIP technology will enable us to construct dependable algorithms to efficiently predict splicing *cis*-elements.

In addition to the phenotypic variability among similar mutations in the same exon, the same mutation often exhibits variable phenotypes, although the variability is usually less (Lund et al. 1996). This is also true for our families. In the Japanese family (F1), two sons (II-1 and II-3) experienced many fractures, whereas the father (I-1) and another son (II-2) had no history of fractures. In the Italian family (F2), the son suffered from many fractures, but his affected mother did not (Mottes et al. 1992). In the Canadian family (F3), the father was classified as OI type IV, whereas his daughter as OI type I (Roschger et al. 2008). Variable clinical phenotypes of the c.3235G>A mutation is likely due to differences in environmental factors or to SNPs in disease-modifying genes, but the molecular bases have not been elucidated in any type of OI.

Molecular basis of hyperuricemia

In F1, hyperuricemia cosegregated with OI type 1. Although no known genes causing hyperuricemia are on chr 17 where *COL1A1* is located, two candidate genes of *PRPSAP1* and *PRPSAP2* are on chr 17. Capillary sequencing of these genes, however, detected no mutation. We thus employed exome-capture resequencing analysis of two siblings in F1 to search for a responsible gene for hyperuricemia. We first looked into SNPs in the 10 candidate genes that are associated with hyperuricemia, purine metabolism and renal excretion, and found 12 SNPs in 10 genes (Table 3). Among them, three SNPs in *ABCG2* (rs2231142) and *SLC22A12* (rs3825016 and rs11231825) are previously reported markers for hyperuricemia and/or gout.

Dehghan et al. (2008) report that rs2231142 in *ABCG2* is associated with gout by a genome-wide association study (OR = 1.74 and 1.71 in white and black participants, respectively). Woodward et al. (2009) showed a significant association between rs2231142 and hyperuricemia (OR = 1.68) in a population-based study of 14,783 individuals. Kolz et al. (2009) demonstrated that rs2231142 elevated the serum urate concentration more strongly in men than in women by meta-analysis of 28,141 individuals. Stark et al. (2009) analyzed 683 patients with gout and indicated a significant association between rs2231142 and gout (OR = 1.37). Although rs2231142 is an attractive causative SNP, our normouricemic subjects were also heterozygous for rs2231142.

Graessler et al. (2006) analyzed 389 German individuals with primary hyperuricemia and found that rs3825016 and rs11231825 in *SLC22A12* were significantly associated with reduced fractional excretion of urate in the kidney. Tabara et al. (2010) analyzed 1,526 normal Japanese individuals retrospectively and longitudinally, and clarified that rs11231825 was associated with reduced urate excretion and with future development of hyperuricemia. Again, although the two SNPs are attractive causes of hyperuricemia, we observe variable dosages of these SNPs even in our normouricemic subjects.

We next looked into neighboring genes of *COL1A1* without considering the functions of the gene products, and identified that two missense variants in *ZPBP2* and *GPATCH8* cosegregated with the *COL1A1* mutation in F1. Neither variant was detected in 300 normal alleles or in dbSNP132. *ZPBP2* p.T69I, however, is unlikely to be pathogenic for three reasons: lack of conservation in mammals; two missense/frameshifting SNPs at or close to the variant site (Fig. 3a); and the benign predicted outcome by PolyPhen-2 and SIFT. On the other hand, p.A979P in *GPATCH8* substitutes an amino acid in the highly conserved serine-rich region (Fig. 3b), and the substitution is predicted to damage the structure and function of the protein by in silico analysis. *GPATCH8* encodes the G patch domain-containing protein 8 that harbors both an RNA-processing domain and a zinc finger domain. *GPATCH8* is expressed in a wide variety of human tissues including skeletal muscles, brain, heart, pancreas, liver and kidney (McKinney et al. 2004). Functions of the *GPATCH8* gene product, however, have not been studied to date. The p.A979P variant in *GPATCH8* is highly likely to be associated with hyperuricemia in F1, but it may also cause another yet unidentified phenotype that cosegregates with OI.

Acknowledgments We would like to thank the families for their participation in this study. We are grateful to Dr. Kunio Ihara at the Center for Gene Research of Nagoya University for the SOLiD sequencing analysis and Keiko Itano for technical assistance. This work was supported by Grants-in-Aid from the Ministry of Education, Culture, Sports, Science and Technology of Japan, and the Ministry of Health, Labor and Welfare of Japan.

References

Adzhubei IA, Schmidt S, Peshkin L, Ramensky VE, Gerasimova A, Bork P, Kondrashov AS, Sunyaev SR (2010) A method and server for predicting damaging missense mutations. Nat Methods 7:248–249

Alanay Y, Avaygan H, Camacho N, Utine GE, Boduroglu K, Aktas D, Alikasifoglu M, Tuncbilek E, Orhan D, Bakar FT, Zabel B, Superti-Furga A, Bruckner-Tuderman L, Curry CJ, Pyott S, Byers PH, Eyre DR, Baldridge D, Lee B, Merrill AE, Davis EC, Cohn DH, Akarsu N, Krakow D (2010) Mutations in the gene encoding the RER protein FKBP65 cause autosomal-recessive osteogenesis imperfecta. Am J Hum Genet 87:572–573

Allen GE, Rogers FB, Lansbury J (1955) Osteogenesis imperfecta tarda with hyperuricemia and gout: report of three cases. Am J Med Sci 230:30–32

Baldridge D, Schwarze U, Morello R, Lennington J, Bertin TK, Pace JM, Pepin MG, Weis M, Eyre DR, Walsh J, Lambert D, Green A, Robinson H, Michelson M, Houge G, Lindman C, Martin J, Ward J, Lemyre E, Mitchell JJ, Krakow D, Rimoin DL, Cohn DH, Byers PH, Lee B (2008) CRTAP and LEPRE1 mutations in recessive osteogenesis imperfecta. Hum Mutat 29:1435–1442

Bodian DL, Madhan B, Brodsky B, Klein TE (2008) Predicting the clinical lethality of osteogenesis imperfecta from collagen glycine mutations. Biochemistry 47:5424–5432

Brunak S, Engelbrecht J, Knudsen S (1991) Prediction of human mRNA donor and acceptor sites from the DNA sequence. J Mol Biol 220:49–65

Cabral WA, Chang W, Barnes AM, Weis M, Scott MA, Leikin S, Makareeva E, Kuznetsova NV, Rosenbaum KN, Tifft CJ, Bulas DI, Kozma C, Smith PA, Eyre DR, Marini JC (2007) Prolyl 3-hydroxylase 1 deficiency causes a recessive metabolic bone disorder resembling lethal/severe osteogenesis imperfecta. Nat Genet 39:359–365

Cartegni L, Chew SL, Krainer AR (2002) Listening to silence and understanding nonsense: exonic mutations that affect splicing. Nat Rev Genet 3:285–298

Cartegni L, Wang J, Zhu Z, Zhang MQ, Krainer AR (2003) ESEfinder: a web resource to identify exonic splicing enhancers. Nucleic Acids Res 31:3568–3571

Christiansen HE, Schwarze U, Pyott SM, AlSwaid A, Al Balwi M, Alrasheed S, Pepin MG, Weis MA, Eyre DR, Byers PH (2010) Homozygosity for a missense mutation in SERPINH1, which encodes the collagen chaperone protein HSP47, results in severe recessive osteogenesis imperfecta. Am J Hum Genet 86:389–398

Constantinou CD, Nielsen KB, Prockop DJ (1989) A lethal variant of osteogenesis imperfecta has a single base mutation that substitutes cysteine for glycine 904 of the alpha 1(I) chain of type I procollagen. The asymptomatic mother has an unidentified mutation producing an overmodified and unstable type I procollagen. J Clin Invest 83:574–584

Dalgleish R (1997) The human type I collagen mutation database. Nucleic Acids Res 25:181–187

Dehghan A, Kottgen A, Yang Q, Hwang SJ, Kao WL, Rivadeneira F, Boerwinkle E, Levy D, Hofman A, Astor BC, Benjamin EJ, van Duijn CM, Witteman JC, Coresh J, Fox CS (2008) Association of three genetic loci with uric acid concentration and risk of gout: a genome-wide association study. Lancet 372:1953–1961

Doring A, Gieger C, Mehta D, Gohlke H, Prokisch H, Coassin S, Fischer G, Henke K, Klopp N, Kronenberg F, Paulweber B, Pfeufer A, Rosskopf D, Volzke H, Illig T, Meitinger T, Wichmann HE, Meisinger C (2008) SLC2A9 influences uric acid concentrations with pronounced sex-specific effects. Nat Genet 40:430–436

Fairbrother WG, Yeh RF, Sharp PA, Burge CB (2002) Predictive identification of exonic splicing enhancers in human genes. Science 297:1007–1013

Gibbs RA, Caskey CT (1987) Identification and localization of mutations at the Lesch–Nyhan locus by ribonuclease A cleavage. Science 236:303–305

Glorieux FH, Rauch F, Plotkin H, Ward L, Travers R, Roughley P, Lalic L, Glorieux DF, Fassier F, Bishop NJ (2000) Type V osteogenesis imperfecta: a new form of brittle bone disease. J Bone Miner Res 15:1650–1658

Glorieux FH, Ward LM, Rauch F, Lalic L, Roughley PJ, Travers R (2002) Osteogenesis imperfecta type VI: a form of brittle bone disease with a mineralization defect. J Bone Miner Res 17:30–38

Goren A, Ram O, Amit M, Keren H, Lev-Maor G, Vig I, Pupko T, Ast G (2006) Comparative analysis identifies exonic splicing regulatory sequences—the complex definition of enhancers and silencers. Mol Cell 22:769–781

Gorlov IP, Gorlova OY, Frazier ML, Amos CI (2003) Missense mutations in hMLH1 and hMSH2 are associated with exonic splicing enhancers. Am J Hum Genet 73:1157–1161

Graessler J, Graessler A, Unger S, Kopprasch S, Tausche AK, Kuhlisch E, Schroeder HE (2006) Association of the human urate transporter 1 with reduced renal uric acid excretion and hyperuricemia in a German Caucasian population. Arthritis Rheum 54:292–300

Hart TC, Gorry MC, Hart PS, Woodard AS, Shihabi Z, Sandhu J, Shirts B, Xu L, Zhu H, Barmada MM, Bleyer AJ (2002) Mutations of the UMOD gene are responsible for medullary cystic kidney disease 2 and familial juvenile hyperuricaemic nephropathy. J Med Genet 39:882–892

Hartikka H, Kuurila K, Korkko J, Kaitila I, Grenman R, Pynnonen S, Hyland JC, Ala-Kokko L (2004) Lack of correlation between the type of COL1A1 or COL1A2 mutation and hearing loss in osteogenesis imperfecta patients. Hum Mutat 24:147–154

Hebsgaard SM, Korning PG, Tolstrup N, Engelbrecht J, Rouze P, Brunak S (1996) Splice site prediction in *Arabidopsis thaliana* pre-mRNA by combining local and global sequence information. Nucleic Acids Res 24:3439–3452

Ishizuka T, Ahmad I, Kita K, Sonoda T, Ishijima S, Sawa K, Suzuki N, Tatibana M (1996) The human phosphoribosylpyrophosphate synthetase-associated protein 39 gene (PRPSAP1) is located in the chromosome region 17q24–q25. Genomics 33:332–334

Katashima R, Iwahana H, Fujimura M, Yamaoka T, Itakura M (1998) Assignment of the human phosphoribosylpyrophosphate synthetase-associated protein 41 gene (PRPSAP2) to 17p11.2–p12. Genomics 54:180–181

Kolz M, Johnson T, Sanna S, Teumer A, Vitart V, Perola M, Mangino M, Albrecht E, Wallace C, Farrall M, Johansson A, Nyholt DR, Aulchenko Y, Beckmann JS, Bergmann S, Bochud M, Brown M, Campbell H, Connell J, Dominiczak A, Homuth G, Lamina C, McCarthy MI, Meitinger T, Mooser V, Munroe P, Nauck M, Peden J, Prokisch H, Salo P, Salomaa V, Samani NJ, Schlessinger D, Uda M, Volker U, Waeber G, Waterworth D, Wang-Sattler R, Wright AF, Adamski J, Whitfield JB, Gyllensten U, Wilson JF, Rudan I, Pramstaller P, Watkins H, Doering A, Wichmann HE, Spector TD, Peltonen L, Volzke H, Nagaraja R, Vollenweider P, Caulfield M, Illig T, Gieger C (2009) Meta-analysis of 28,141 individuals identifies common variants within five new loci that influence uric acid concentrations. PLoS Genet 5:e1000504

Kumar P, Henikoff S, Ng PC (2009) Predicting the effects of coding non-synonymous variants on protein function using the SIFT algorithm. Nat Protoc 4:1073–1081

Lalonde E, Albrecht S, Ha KC, Jacob K, Bolduc N, Polychronakos C, Dechelotte P, Majewski J, Jabado N (2010) Unexpected allelic heterogeneity and spectrum of mutations in Fowler syndrome revealed by next-generation exome sequencing. Hum Mutat 31:918–923

Langmead B, Trapnell C, Pop M, Salzberg SL (2009) Ultrafast and memory-efficient alignment of short DNA sequences to the human genome. Genome Biol 10:R25

Lapunzina P, Aglan M, Temtamy S, Caparros-Martin JA, Valencia M, Leton R, Martinez-Glez V, Elhossini R, Amr K, Vilaboa N, Ruiz-Perez VL (2010) Identification of a frameshift mutation in Osterix in a patient with recessive osteogenesis imperfecta. Am J Hum Genet 87:110–114

Licatalosi DD, Mele A, Fak JJ, Ule J, Kayikci M, Chi SW, Clark TA, Schweitzer AC, Blume JE, Wang X, Darnell JC, Darnell RB (2008) HITS-CLIP yields genome-wide insights into brain alternative RNA processing. Nature 456:464–469

Lund AM, Schwartz M, Skovby F (1996) Variable clinical expression in a family with OI type IV due to deletion of three base pairs in COL1A1. Clin Genet 50:304–309

Lund AM, Skovby F, Schwartz M (1997) Serine for glycine substitutions in the C-terminal third of the alpha 1(I) chain of collagen I in five patients with nonlethal osteogenesis imperfecta. Hum Mutat 9:378–382

Marini JC, Forlino A, Cabral WA, Barnes AM, San Antonio JD, Milgrom S, Hyland JC, Korkko J, Prockop DJ, De Paepe A, Coucke P, Symoens S, Glorieux FH, Roughley PJ, Lund AM, Kuurila-Svahn K, Hartikka H, Cohn DH, Krakow D, Mottes M, Schwarze U, Chen D, Yang K, Kuslich C, Troendle J, Dalgleish R, Byers PH (2007) Consortium for osteogenesis imperfecta mutations in the helical domain of type I collagen: regions rich in lethal mutations align with collagen binding sites for integrins and proteoglycans. Hum Mutat 28:209–221

McKinney JL, Murdoch DJ, Wang J, Robinson J, Biltcliffe C, Khan HM, Walker PM, Savage J, Skerjanc I, Hegele RA (2004) Venn analysis as part of a bioinformatic approach to prioritize expressed sequence tags from cardiac libraries. Clin Biochem 37:953–960

Morello R, Bertin TK, Chen Y, Hicks J, Tonachini L, Monticone M, Castagnola P, Rauch F, Glorieux FH, Vranka J, Bachinger HP, Pace JM, Schwarze U, Byers PH, Weis M, Fernandes RJ, Eyre DR, Yao Z, Boyce BF, Lee B (2006) CRTAP is required for prolyl 3-hydroxylation and mutations cause recessive osteogenesis imperfecta. Cell 127:291–304

Mottes M, Sangalli A, Valli M, Gomez Lira M, Tenni R, Buttitta P, Pignatti PF, Cetta G (1992) Mild dominant osteogenesis imperfecta with intrafamilial variability: the cause is a serine for glycine alpha 1(I) 901 substitution in a type-I collagen gene. Hum Genet 89:480–484

Ng SB, Turner EH, Robertson PD, Flygare SD, Bigham AW, Lee C, Shaffer T, Wong M, Bhattacharjee A, Eichler EE, Bamshad M, Nickerson DA, Shendure J (2009) Targeted capture and massively parallel sequencing of 12 human exomes. Nature 461:272–276

Ng SB, Bigham AW, Buckingham KJ, Hannibal MC, McMillin MJ, Gildersleeve HI, Beck AE, Tabor HK, Cooper GM, Mefford HC, Lee C, Turner EH, Smith JD, Rieder MJ, Yoshiura K, Matsumoto N, Ohta T, Niikawa N, Nickerson DA, Bamshad MJ, Shendure J (2010a) Exome sequencing identifies MLL2 mutations as a cause of Kabuki syndrome. Nat Genet 42:790–793

Ng SB, Buckingham KJ, Lee C, Bigham AW, Tabor HK, Dent KM, Huff CD, Shannon PT, Jabs EW, Nickerson DA, Shendure J,

Bamshad MJ (2010b) Exome sequencing identifies the cause of a Mendelian disorder. Nat Genet 42:30–35

Ohno K, Milone M, Shen X-M, Engel AG (2003) A frameshifting mutation in *CHRNE* unmasks skipping of the preceding exon. Hum Mol Genet 12:3055–3066

Rauch F, Glorieux FH (2004) Osteogenesis imperfecta. Lancet 363:1377–1385

Reese MG, Eeckman FH, Kulp D, Haussler D (1997) Improved splice site detection in Genie. J Comput Biol 4:311–323

Roessler BJ, Nosal JM, Smith PR, Heidler SA, Palella TD, Switzer RL, Becker MA (1993) Human X-linked phosphoribosylpyrophosphate synthetase superactivity is associated with distinct point mutations in the PRPS1 gene. J Biol Chem 268:26476–26481

Roschger P, Fratzl-Zelman N, Misof BM, Glorieux FH, Klaushofer K, Rauch F (2008) Evidence that abnormal high bone mineralization in growing children with osteogenesis imperfecta is not associated with specific collagen mutations. Calcif Tissue Int 82:263–270

Sillence DO, Senn A, Danks DM (1979) Genetic heterogeneity in osteogenesis imperfecta. J Med Genet 16:101–116

Stark K, Reinhard W, Grassl M, Erdmann J, Schunkert H, Illig T, Hengstenberg C (2009) Common polymorphisms influencing serum uric acid levels contribute to susceptibility to gout, but not to coronary artery disease. PLoS One 4:e7729

Tabara Y, Kohara K, Kawamoto R, Hiura Y, Nishimura K, Morisaki T, Kokubo Y, Okamura T, Tomoike H, Iwai N, Miki T (2010) Association of four genetic loci with uric acid levels and reduced renal function: the J-SHIPP Suita study. Am J Nephrol 32:279–286

van Dijk FS, Nesbitt IM, Zwikstra EH, Nikkels PG, Piersma SR, Fratantoni SA, Jimenez CR, Huizer M, Morsman AC, Cobben JM, van Roij MH, Elting MW, Verbeke JI, Wijnaendts LC, Shaw NJ, Hogler W, McKeown C, Sistermans EA, Dalton A, Meijers-Heijboer H, Pals G (2009) PPIB mutations cause severe osteogenesis imperfecta. Am J Hum Genet 85:521–527

Vitart V, Rudan I, Hayward C, Gray NK, Floyd J, Palmer CN, Knott SA, Kolcic I, Polasek O, Graessler J, Wilson JF, Marinaki A, Riches PL, Shu X, Janicijevic B, Smolej-Narancic N, Gorgoni B, Morgan J, Campbell S, Biloglav Z, Barac-Lauc L, Pericic M, Klaric IM, Zgaga L, Skaric-Juric T, Wild SH, Richardson WA, Hohenstein P, Kimber CH, Tenesa A, Donnelly LA, Fairbanks LD, Aringer M, McKeigue PM, Ralston SH, Morris AD, Rudan P, Hastie ND, Campbell H, Wright AF (2008) SLC2A9 is a newly identified urate transporter influencing serum urate concentration, urate excretion and gout. Nat Genet 40:437–442

Wang Z, Rolish ME, Yeo G, Tung V, Mawson M, Burge CB (2004) Systematic identification and analysis of exonic splicing silencers. Cell 119:831–845

Ward LM, Rauch F, Travers R, Chabot G, Azouz EM, Lalic L, Roughley PJ, Glorieux FH (2002) Osteogenesis imperfecta type VII: an autosomal recessive form of brittle bone disease. Bone 31:12–18

Woodward OM, Kottgen A, Coresh J, Boerwinkle E, Guggino WB, Kottgen M (2009) Identification of a urate transporter, ABCG2, with a common functional polymorphism causing gout. Proc Natl Acad Sci USA 106:10338–10342

Yeo GW, Coufal NG, Liang TY, Peng GE, Fu XD, Gage FH (2009) An RNA code for the FOX2 splicing regulator revealed by mapping RNA–protein interactions in stem cells. Nat Struct Mol Biol 16:130–137

Yi X, Liang Y, Huerta-Sanchez E, Jin X, Cuo ZX, Pool JE, Xu X, Jiang H, Vinckenbosch N, Korneliussen TS, Zheng H, Liu T, He W, Li K, Luo R, Nie X, Wu H, Zhao M, Cao H, Zou J, Shan Y, Li S, Yang Q, Asan Ni P, Tian G, Xu J, Liu X, Jiang T, Wu R, Zhou G, Tang M, Qin J, Wang T, Feng S, Li G, Huasang Luosang J, Wang W, Chen F, Wang Y, Zheng X, Li Z, Bianba Z, Yang G, Wang X, Tang S, Gao G, Chen Y, Luo Z, Gusang L, Cao Z, Zhang Q, Ouyang W, Ren X, Liang H, Zheng H, Huang Y, Li J, Bolund L, Kristiansen K, Li Y, Zhang Y, Zhang X, Li R, Li S, Yang H, Nielsen R, Wang J, Wang J (2010) Sequencing of 50 human exomes reveals adaptation to high altitude. Science 329:75–78

Zhang XH, Chasin LA (2004) Computational definition of sequence motifs governing constitutive exon splicing. Genes Dev 18:1241–1250

Zhang XH, Kangsamaksin T, Chao MS, Banerjee JK, Chasin LA (2005) Exon inclusion is dependent on predictable exonic splicing enhancers. Mol Cell Biol 25:7323–7332

Anti-MuSK autoantibodies block binding of collagen Q to MuSK

Y. Kawakami, BSc
M. Ito, PhD
M. Hirayama, MD, PhD
K. Sahashi, MD, PhD
B. Ohkawara, PhD
A. Masuda, MD, PhD
H. Nishida, MD, PhD
N. Mabuchi, MD, PhD
A.G. Engel, MD
K. Ohno, MD, PhD

Address correspondence and reprint requests to Dr. Ohno, Division of Neurogenetics, Center for Neurological Diseases and Cancer, Nagoya University Graduate School of Medicine, 65 Tsurumai, Showa-ku, Nagoya 466-8550, Japan
ohnok@med.nagoya-u.ac.jp

ABSTRACT

Objective: Muscle-specific receptor tyrosine kinase (MuSK) antibody-positive myasthenia gravis (MG) accounts for 5%–15% of autoimmune MG. MuSK mediates the agrin-signaling pathway and also anchors the collagenic tail subunit (ColQ) of acetylcholinesterase (AChE). The exact molecular target of MuSK–immunoglobulin G (IgG), however, remains elusive. As acetylcholine receptor (AChR) deficiency is typically mild and as cholinesterase inhibitors are generally ineffective, we asked if MuSK-IgG interferes with binding of ColQ to MuSK.

Methods: We used 3 assays: in vitro overlay of the human ColQ-tailed AChE to muscle sections of *Colq*−/− mice; in vitro plate-binding assay to quantitate binding of MuSK to ColQ and to LRP4; and passive transfer of MuSK-IgG to mice.

Results: The in vitro overlay assay revealed that MuSK-IgG blocks binding of ColQ to the neuromuscular junction. The in vitro plate-binding assay showed that MuSK-IgG exerts a dose-dependent block of MuSK binding to ColQ by but not to LRP4. Passive transfer of MuSK-IgG to mice reduced the size and density of ColQ to ~10% of controls and had a lesser effect on the size and density of AChR and MuSK.

Conclusions: As lack of ColQ compromises agrin-mediated AChR clustering in *Colq*−/− mice, a similar mechanism may lead to AChR deficiency in MuSK-MG patients. Our experiments also predict partial AChE deficiency in MuSK-MG patients, but AChE is not reduced in biopsied NMJs. In humans, binding of ColQ to MuSK may be dispensable for clustering ColQ, but is required for facilitating AChR clustering. Further studies will be required to elucidate the basis of this paradox. ***Neurology*® 2011;77:1819–1826**

GLOSSARY

AChE = acetylcholinesterase; **AChR** = acetylcholine receptor; **ColQ** = collagen Q; **IgG** = immunoglobulin G; **LRP4** = low-density lipoprotein receptor-related protein 4; **MG** = myasthenia gravis; **MuSK** = muscle-specific receptor tyrosine kinase; **NMJ** = neuromuscular junction; **SDS-PAGE** = sodium dodecyl sulfate–polyacrylamide gel electrophoresis.

During development of the neuromuscular junction (NMJ), neural agrin released from the nerve terminal binds to the postsynaptic transmembrane protein LRP4.[1,2] Dimerized LRP4 forms a heterotetramer with the dimerized muscle-specific receptor tyrosine kinase (MuSK).[3] MuSK together with Dok-7 promotes clustering of acetylcholine receptor (AChR) on the junctional folds by rapsyn.[4] The clustering effect of MuSK is mediated by distinct pathways involving Rho GTPase.[5]

Editorial, page 1783

At the NMJ, 3 tetramers of catalytic subunits of acetylcholinesterase (AChE) are linked to ColQ, the triple helical collagenic subunit.[6] ColQ-tailed AChE is anchored to the synaptic basal lamina by 2 mechanisms: 2 sets of heparan sulfate proteoglycan residues in the collagen

Supplemental data at www.neurology.org

Supplemental Data

From the Division of Neurogenetics (Y.K., M.I., B.O., A.M., K.O.), Center for Neurological Diseases and Cancer, Nagoya University Graduate School of Medicine, Nagoya; Department of Pathophysiological Laboratory Sciences (M.H.), Nagoya University Graduate School of Medicine, Nagoya; Department of Neurology (K.S.), Aichi Medical University, Aichi; Department of Neurology (H.N.), Gifu Prefectural General Medical Center, Gifu; Department of Neurology (N.M.), Okazaki City Hospital, Okazaki, Japan; and Department of Neurology (A.G.E.), Mayo Clinic, Rochester, MN.

Study funding: Supported by a Grant-in-Aid from the Ministry of Education, Culture, Sports, Science, and Technology of Japan; a Grant-in-Aid from the Ministry of Health, Labor, and Welfare of Japan; a research grant from the National Institute of Neurological Disorders and Stroke (NS6277); and a research grant from the Muscular Dystrophy Association.

Disclosure: Author disclosures are provided at the end of the article.

domain of ColQ[7] bind to heparin sulfate proteoglycans, such as perlecan[8]; and the C-terminal domain of ColQ binds to MuSK.[9]

Five percent to 15% of patients with myasthenia gravis (MG) carry antibodies against MuSK (MuSK–immunoglobulin G [IgG]).[10,11] MuSK-MG patients respond favorably to immunotherapy, but usually do not respond to, or are even worsened by, cholinesterase inhibitors.[12–15] Anti-AChR antibodies comprise IgG1 and IgG3 moieties that bind complement whereas anti-MuSK antibodies are largely IgG4 that do not activate complement, and complement deposits at the NMJ are sparse.[16–18] However, the exact target of MuSK-IgG remains elusive. We therefore examined an effect of MuSK-IgG on an interaction between ColQ and MuSK by in vitro and in vivo assays, and found that MuSK-IgG blocks this interaction.

METHODS

Patients. We obtained serum from 4 MuSK-MG patients (patients 1–4) and a patient with limb-girdle muscular dystrophy as a control (control 1). We obtained 10 mL peripheral blood from patients 1, 3, 4, and control and residual plasmapheresis fluid from patient 2. We also obtained expired fresh-frozen plasma (control 2) from Dr. Isao Takahashi at the Aichi Red Cross Blood Center with institutional approval. We used sera of patient 2 and control 2 for all the experiments, and sera of patients 1, 3, 4, and control 1 only for the in vitro overlay and in vitro plate binding assays because only small amounts of sera were available from these patients.

Ages and genders of patients 1–4 were a 48-year-old woman, a 30-year-old woman, a 59-year-old man, and a 45-year-old woman, respectively. The titers of anti-MuSK antibodies of patients 1–3 were 22.0 nM, 11.2 nM, and 0.12 nM, respectively (normal <0.01 nM). Patient 4 was positive for anti-MuSK antibody, but the titer was not determined.

Standard protocol approvals, registrations, and patient consents. We performed all human studies under the institutional review board approvals of the Nagoya University Graduate School of Medicine and the Mayo Clinic, and obtained written informed consents from each patient and a control. We also obtained approvals of the *Colq*−/− mice studies and the passive IgG transfer studies by the Animal Care and Use Committee of the Nagoya University.

Plasmids. We previously made CMV-based mammalian expression vectors, pTargeT-*COLQ* and pTargeT-*ACHE*.[19] To generate hMuSKect-myc, we cloned the extracellular domain (aa 1–393) of human *MUSK* cDNA (Open Biosystems) into a mammalian expression vector pAPtag-5 (GenHunter) at the *Nhe*I and *Xho*I sites upstream of a myc epitope. For hLRP4N-FLAG, we cloned the extracellular domain (aa 1–1722) of human *LRP4* cDNA (Open Biosystems) into the *Hin*dIII and *Xba*I sites upstream of a 3xFLAG epitope of a mammalian expression vector p3XFLAG-CMV-14 (Sigma Aldrich).

Preparation of recombinant human ColQ-tailed AChE. We prepared human ColQ-tailed AChE for in vitro overlay assay and for in vitro plate-binding assay. Both pTargeT-*COLQ* and pTargeT-*ACHE* were transfected into HEK293 cells in a 10-cm dish using the calcium phosphate method as described elsewhere.[20] We extracted proteins from the cells in Tris-HCl buffer (50 mM Tris-HCl [pH 7.0], 0.5% Triton X-100, 0.2 mM EDTA, leupeptin [2 μg/mL], and pepstatin [1 μg/mL]) containing 1 M NaCl, and diluted the extracts containing ColQ-tailed AChE in Tris-HCl buffer containing 0.2 M NaCl and loaded onto the HiTrap Heparin HP columns (GE Healthcare). We washed the columns with 5 volumes of Tris-HCl buffer containing 0.2 M NaCl, and eluted ColQ-tailed AChE with Tris-HCl buffer containing 1 M NaCl. We concentrated the eluate with an Amicon Ultra-4 Centrifugal Filter (50K) (Millipore) to 12-Ellman units per mL. The units were normalized with the Torpedo-derived AChE (C2888, Sigma-Aldrich).

Preparation of hMuSKect-myc and hLRP4N-FLAG proteins. We prepared hMuSKect-myc and hLRP4N-FLAG for in vitro plate-binding assays. We introduced a construct carrying either hMuSKect-myc or hLRP4N-FLAG into HEK293 cells in a 10-cm dish using the calcium phosphate method as above. We purified the hMuSKect-myc with the c-myc-Tagged Protein Mild Purification Kit version 2 (MBL), and purified the hLRP4N-FLAG with the Anti-DYKDDDDK-tag Antibody Beads (Wako). We detected purified hMuSKect-myc and hLRP4N-FLAG by anti-myc antibody (9E10, Abcam) and anti-FLAG antibody (M2, Sigma-Aldrich), respectively (data not shown), and also detected hMuSKect-myc by sodium dodecyl sulfate–polyacrylamide gel electrophoresis (SDS-PAGE) followed by protein staining with the Oriole Fluorescent Gel Stain (Bio-Rad).

Purification of plasma IgG. We purified IgG as described elsewhere[21] with minor modifications. We adjusted plasma to pH 8.0 with 1 M NaOH. While stirring 1 volume of plasma, we slowly added 3.5 volumes of 0.4% rivanol (Tokyo Chemical Industries) in water for 30 minutes. We left the solution overnight at RT, and removed a tenacious yellow precipitate. After filtering the supernatant through Whatman no. 1 paper to remove residual precipitates, we added 8 g of activated charcoal (Wako Chemicals) for 100 mL of the IgG solution and incubated overnight at 4°C to remove rivanol. We then slowly added an equal amount of saturated ammonium sulfate, and again incubated overnight at RT to precipitate crude IgG. We centrifuged the solution at 3,000 × *g* for 30 minutes, and added saline to the precipitate to form a slurry, which was then transferred to a dialysis tube (Spectra/Por MWCO 50,000, Spectrum Laboratories). We dialyzed the solution in saline at 4°C for 3 hours, followed by dialysis in PBS at 4°C for 2 hours and then overnight. We removed residual charcoals by filtering through a 0.22-μm Millex-GP filter (Millipore), and concentrated IgG using Amicon Ultra 50K (Millipore). We confirmed purity of isolated IgG by 6% SDS-PAGE under a nonreducing condition. We also reduced IgG in 4% 2-mercaptoethanol and fractionated the heavy and light chains by 10% SDS-PAGE.

Incubation of purified IgG to a muscle section of *Colq*−/− mice. We prepared 10-μm-thick sections of quadriceps muscles of *Colq*−/− mice[22] with a Leica CW3050–4 cryostat at −20°C. We blocked nonspecific binding of a muscle section with the blocking buffer that contained 5% sheep serum in PBS at RT for 2 hours. We suspended the purified IgG in the blocking buffer at 50 μg/mL, and overlaid it on a muscle section at 4°C overnight. We detected human IgG by FITC-labeled

anti-human IgG antibody (02–10-06, KPL), and AChR by Alexa594-labeled α-bungarotoxin (Molecular Probes).

In vitro overlay assay. The overlay binding method was essentially as previously described.[23] We overlaid 600 μg IgG of patients at 4°C overnight before adding 120-milli-Ellman units of ColQ-tailed AChE.

In vitro plate-binding assay for quantifying ColQ-MuSK interaction. We coated the Maxi-Sorp Immuno Plate (Nunc) with 0.15 μg of purified hMuSKect-myc at 4°C overnight and then incubated it with a blocking buffer that contained 50 mM Tris-HCl (pH 7.4), 0.5% BSA, 0.5% ovalbumin, and 0.5 M NaCl at RT for 1 hour. We incubated the wells with 1 pg to 100 μg of IgG of controls 1 and 2 and patients 1–4 at 4°C for 6 hours. We added 0.12-Ellman units of ColQ-tailed AChE as described above. We then quantified the bound ColQ-tailed AChE by the Ellman method in the presence of 5×10^{-5} M ethopropazine.[19] Each time before we moved to the next step, we washed the plate 3 times with PBS.

In vitro plate-binding assay for quantifying LRP4-MuSK interaction. We coated the Maxi-Sorp Immuno Plate with 0.15 μg of purified hMuSKect-myc as described above, and then blocked with 1% BSA in PBS at RT for 1 hour. We incubated the wells with 1 pg to 100 μg of IgG of control 2 and patient 2 at 4°C for 6 hours. We added 0.12 μg of purified hLRP4N-FLAG on each well at RT for 2 hours. We then quantified the bound hLRP4N-FALG by anti-FLAG-HRP using the TMB substrate kit (Pierce). Again, between each step, we washed the plates 3 times with PBS.

Passive transfer of human IgG to mice. We made passive transfer model mice as described elsewhere.[24] We intraperitoneally injected 40 mg IgG of control 2 and patient 2 into 6-week-old female C57BL/6J mice every day for 15 days. We sterilized IgG with a 0.22-μm filter (Millipore) and dissolved it in 400 μL PBS. The mice were killed on day 16 under deep anesthesia. To suppress any active immune response to the human protein,[25] we injected 300 mg/kg of cyclophosphamide monohydrate (10 mg/mL in 0.9% NaCl) intraperitoneally 24 hours after the first IgG injection. We also injected IgG of patient 2 into 2 additional mice to confirm consistency, and analyzed a representative mouse in detail. We detected AChR by Alexa594-labeled α-bungarotoxin (Molecular Probes), ColQ by 1:100 of a newly raised anti-ColQ antibody (figure e-1 on the *Neurology*® Web site at www.neurology.org), and MuSK by 1:100 of anti-MuSK antibody (C-19, Santa Cruz). We quantified signals by the BZ-9000 microscope (Keyence) equipped with the Dynamic Cell Count software BZ-H1C (Keyence).

Figure 1 **Muscle-specific receptor tyrosine kinase (MuSK)-immunoglobulin G (IgG) recognizes the neuromuscular junction (NMJ) of *Colq*−/− mice**

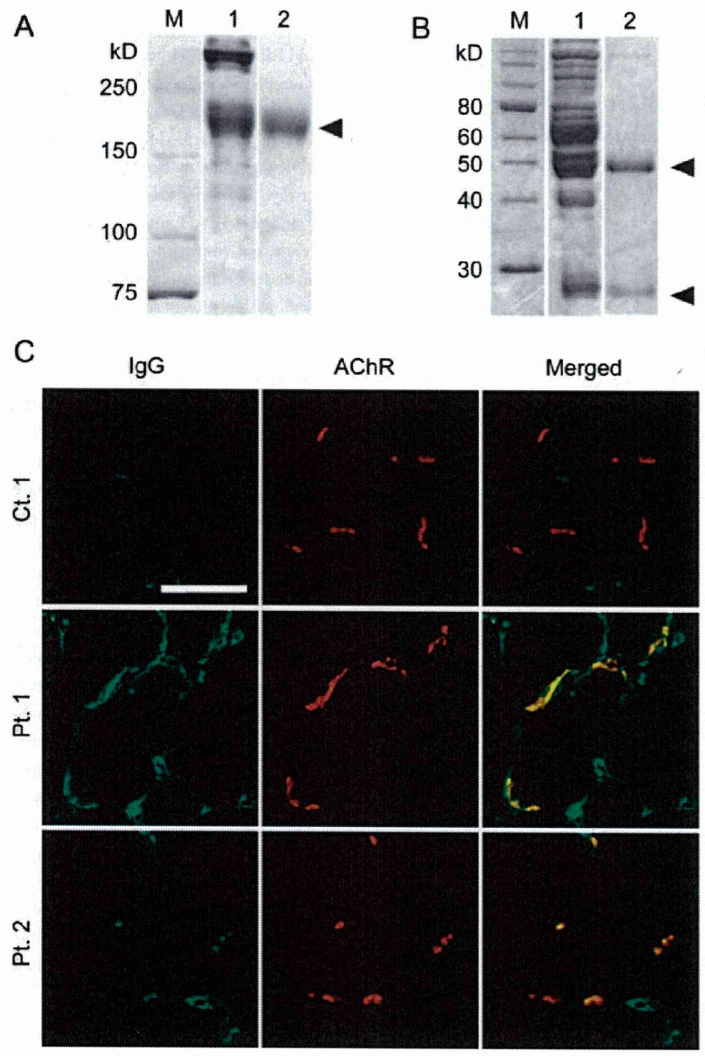

Nonreducing (A) and reducing (B) sodium dodecyl sulfate–polyacrylamide gel electrophoresis of serum proteins and purified IgG of patient 1. Gels are stained with Coomassie brilliant blue. M = molecular weight markers; 1 = serum before purification; 2 = purified IgG. Arrowheads point to IgG of 160 kD (A), as well as the heavy (50 kD) and light (25 kD) chains of IgG (B). (C) In vitro overlay of purified IgG on a 10-μm skeletal muscle section of *Colq*−/− mice. IgG is visualized with FITC-labeled antihuman IgG and acetylcholine receptor with Alexa594-labeled α-bungarotoxin. Scale bar = 50 μm.

RESULTS **MuSK-IgG recognizes NMJ of a muscle section of *Colq*−/− mouse.** We first confirmed that human MuSK-IgG recognizes the mouse NMJ. We isolated IgG from serum of MuSK-MG patients and confirmed the purity of IgG by Coomassie staining of nonreducing (figure 1A) and reducing (figure 1B) SDS-PAGEs. We then overlaid MuSK-IgG on quadriceps muscle sections of *Colq*−/− mice.[22] IgG of control 1 was not bound to the NMJ, whereas IgGs of patients 1 and 2 colocalized to the NMJs (figure 1C). Human MuSK-IgG thus has the potential to bind to the mouse NMJ.

In vitro overlay assay discloses that MuSK-IgG blocks binding of ColQ-tailed AChE to the NMJ of a muscle section of *Colq*−/− mouse. We previously demonstrated that the purified recombinant human ColQ-tailed AChE protein complex could bind to sections of the frog NMJs[23] and the mouse NMJs (in preparation) in vitro. Using the in vitro overlay assay, we next examined whether MuSK-IgG blocks anchoring of ColQ-tailed AChE to the mouse NMJs. We incubated a muscle section of *Colq*−/− mice with MuSK-IgG overnight at 4°C and overlaid human ColQ-tailed AChE followed by histologic visualization of ColQ and AChR (figure 2). In the presence of

Figure 2 **In vitro overlay assays**

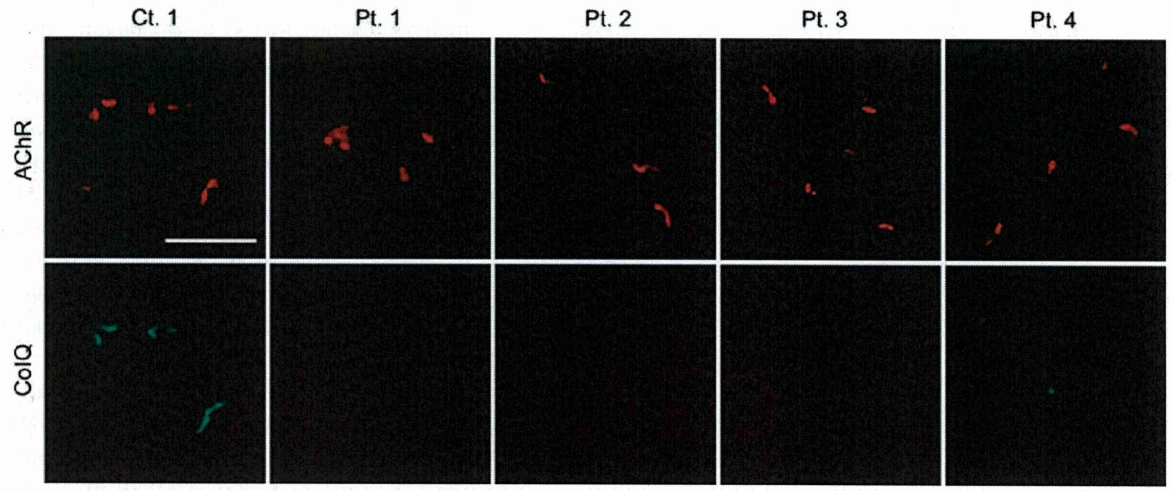

Purified recombinant collagen Q (ColQ)-tailed acetylcholinesterase (AChE) was overlaid on a 10-μm quadriceps muscle section of *Colq*−/− mice in the presence of the indicated purified muscle-specific receptor tyrosine kinase-immunoglobulin G. ColQ is stained with anti-ColQ antibody and acetylcholine receptor (AChR) with Alexa594-labeled α-bungarotoxin. Scale bar = 50 μm.

IgG of control 1, ColQ was colocalized with AChRs, whereas, in the presence of 4 MuSK-IgGs, no ColQ signal was observed at the NMJs.

In vitro plate-binding assay shows that MuSK-IgG blocks binding of ColQ-tailed AChE but not of LRP4 to MuSK. We next quantified an effect of MuSK-IgG on an interaction of human ColQ and human MuSK by an in vitro plate-binding assay. We synthesized and purified the myc-tagged extracellular domain of human MuSK (hMuSKect-myc). We then incubated an hMuSKect-coated plate with variable concentrations of control IgG or MuSK-IgG, and added a fixed amount of the purified recombinant human ColQ-tailed AChE. In 2 controls, AChE remained bound even in the presence of 100 μg of IgG, whereas in 4 MuSK-MG patients the numbers of bound AChE were proportionally decreased with increasing amounts of the patient's IgG (figure 3A).

We also examined the effect of MuSK-IgG on the interaction between the extracellular domain of MuSK and LRP4. We found that even at 100 μg IgG of control 2 or patient 2 did not block binding of LRP4 to MuSK (figure 3B).

Passive transfer model exhibits reduced ColQ signals at the NMJs. As described in the introduction, active and passive immunization of model animals reveals reduction of AChRs at the NMJs,[24,26–29] but an effect of MuSK-IgG on ColQ-tailed AChE has not been examined to date. We thus injected IgG of control 2 and patient 2 for 14 days to C57BL/6J female mice and visualized the expression of AChR, ColQ, MuSK, and AChE in quadriceps muscle sections. Signal intensities of ColQ and AChE were markedly attenuated, but the AChR and MuSK signal intensities were only moderately reduced (figure 4, A and B). Quantitative analysis of the fluorescence signals revealed that signal areas (figure 4C), intensities (figure 4D), and densities (figure 4E) of ColQ in mice injected with patient 2 IgG were significantly reduced. Conversely, signal areas (figure 4C), intensities (figure 4D), and densities (figure 4E) of AChR were only moderately reduced. Similarly, the same parameters of the MuSK signal were moderately reduced (figure 4, C, D, and E). Moderate reductions of the areas and intensities of AChR and MuSK signals are likely due to reduced sizes of the NMJs, because the densities of AChR and MuSK were only marginally affected. In addition, whereas the number of MuSK per AChR remained essentially the same, the number of ColQ per AChR was prominently reduced (figure 4F). To summarize, MuSK-IgG compromised anchoring of ColQ-tailed AChE and had a less prominent effect on the expression of MuSK and AChR.

DISCUSSION Molecular basis of MuSK-MG has been examined in cultured cells[30,31] as well as in active[28,29] and passive[24,26,27] immunization models. Application of MuSK-MG antibodies to TE671 muscle cells induces inhibition of cell proliferation and secondarily leads to downregulation of AChR and rapsyn.[30] Similarly, MuSK-MG antibodies have no or minimal effect on the cell surface expression of AChR in TE671 and C2C12 muscle cells.[31] Conversely, mice[29] and rabbits[28] immunized with recombinant MuSK develop myasthenic symptoms and